2019

Controlled cavitation design and investigation of its effect in traumatic-brain injuries

Alex Wrede
Iowa State University

Controlled cavitation design and investigation of its effect in traumatic-brain injuries

by

Alex Wrede

A dissertation submitted to the graduate faculty

in partial fulfillment of the requirements for the degree of

DOCTOR OF PHILOSOPHY

Major: Mechanical Engineering

Program of Study Committee:
Nicole Hashemi, Major Professor
Reza Montazami
Travis Sippel
Timothy Bigelow
Donald Sakaguchi

The student author, whose presentation of the scholarship herein was approved by the program of study committee, is solely responsible for the content of this dissertation. The Graduate College will ensure this dissertation is globally accessible and will not permit alterations after a degree is conferred.

Iowa State University

Ames, Iowa

2019

DEDICATION

This dissertation is dedicated to my cherished family:

My Wife:

Josie Wrede

My parents:

Dan & Jane Wrede

All immediate and extended family and friends

for their relentless love, support, and encouragement.

TABLE OF CONTENTS

LIST OF FIGURES

Page

NOMENCLATURE

CSF	Cerebrospinal Fluid
MB	Microbubble
PBS	Phosphate-Buffered Saline
PCL	Polycaprolactone
PDMS	Polydimethylsiloxane
qPCR	Quantitative Polymerase Chain Reaction
TBI	Traumatic Brain Injury

ACKNOWLEDGMENTS

I would like to thank my major professor, Dr. Nicole Hashemi, and my committee members, Dr. Reza Montazami, Dr. Travis Sippel, Dr. Timothy Bigelow, and Dr. Donald Sakaguchi, for their guidance through the duration of this research.

In addition, I would also like to thank all my current and former lab mates, department faculty and staff, and mentee students for their time and help on various parts of this research. Thank you to Marilyn McNamara and Rajeendra Pemathilaka, who have helped me tremendously throughout multiple facets of this project. I want to also offer my appreciation to Curtis Mosher for assistance and training with 3D Confocal Microscopy techniques. I thank Dan Barnard for his help with ultrasonics, Bhavika Patel for her assistance with cell culture techniques, Stuart Barkley for his help with optics, Jie Luo for his help with biology and qPCR techniques, and RITEC, Inc. for lending a RAM-5000 power amplification system.

This work was partially supported by the Office of Naval Research (ONR) Grant N000141612246, ONR Grant N000141712620, and Iowa State University.

ABSTRACT

Traumatic brain injuries (TBIs) are a highly complex injury that is heavily studied in modern research. An aspect of TBIs that has been almost entirely overlooked is the existence of cavitation in the brain during a high impact injury. The presence of cavitation in the brain is a recent theory and is feared to cause detrimental damages on brain tissue. The following chapters aim to investigate this phenomena by first engineering an apparats that simulates controlled cavitation for TBI applications. The apparatus that is used in this study involves acoustical techniques to cause microbubbles (MBs) to oscillate and fragment under resonant conditions, detailed in Chapter 2. MBs are created by using a syringe to push air through capillary tubing, resulting in MBs ranging from 50-100 μm. The MBs exit at a consistent rate and arbitrary amounts are adhered to an analyt sample prior to inducing acoustical cavitation. This method is advantageous and novel because it allows for arbitrary amounts of cavitation, the size of the created MBs is similar to that of what is thought to exist *in vivo,* and it is cost-effective.

Using this developed apparatus, there are a variety of studies that have novel potential. Chapter 3 highlights the response the soft polymers have to surrounding cavitation. Using 3D confocal microscopy and interferometry techniques, it is apparent that the soft polymer surface is visually damaged after cavitation exposure. Further roughness calculations demonstrate distinct alterations in the overall roughness and skewness of the surface for experimental samples. Although these soft polymers do not entirely replicate the response to cavitation of the human brain, they provide insight on how alarming inter-cranial actually is and motivate future studies.

Reactive astrocytes are known to have a large role in the response of the brain after a TBI. Introducing astrocytes in the developed apparatus is made possible by sterilizing all the components and using phosphate buffered saline (PBS) as the cavitation medium. Culturing

astrocytes on biocompatible microfibers allows for the investigation of a finite amount of cells. Chapter 4 illustrates a distinct morphological change that the astrocytes undergo after experiencing cavitation. Over 48 hours different stages of morphology are represented. Chapter 4 also elucidates genetic changes that astrocytes undergo immediately after cavitation, via quantitative polymerase chain reaction (qPCR) techniques. Results show alarming upregulation in various genes that are known to be upregulated in other neurodegenerative diseases. These findings add additional concern for the damages that cavitation causes on nearby cranial anatomy. These results also inspired an additional genetic study to characterize the longitudinal gene expression trend from 0-48 hours post-cavitation, summarized in Chapter 5. This was primarily an exploratory study to help further investigate the morphological changes that were found in Chapter 4. In the ten genes that were studied, there was no consistent trend in gene expression from multiple genes to the next. Future studies aim to include RNA sequencing to obtain a complete summary on the expression changes in the entire genome.

Taken together, the following chapters summarize the engineering of an applied apparatus that simulates controlled cavitation *in vitro*. Introducing soft polymers in this apparatus yields distinct surface alterations. This apparatus is biocompatible and used to study morphological and genetic changes in astrocytes. These results are novel and help legitimize the concerning detriments that cavitation has inside the human skull. Future studies aim to build on this foundation and continue to bolster the current understanding, therapeutics, and preventative techniques in TBIs.

CHAPTER 1. INTRODUCTION: CAVITATION PRODUCTION METHODS AND NEURONAL RESPONSE TO TBI

1.1 Cavitation Terminology and Applications

Cavitation is defined as the rapid growth and collapse of MBs in low pressure regions. Cavitation has been studied for many decades and has been documented to exist in numerous applications. First, in watercraft propulsion systems cavitation has been proven to exist in the low pressure regions of a spinning propeller [1]. Second, cavitation has been proven to exist in hydrodynamic pumping applications. When there is a change of piping diameter there is a low pressure region downstream of the diameter change for cavitation to form when flow is introduced [2]. Also, MBs have been used to carry drugs to different areas of the body and when they arrive to an arbitrary destination they are fragmented, releasing the particular drugs and creating cavitation [3, 4]. Recent studies have concluded the existence of cavitation in the skull during a TBI [5-7]. During a TBI, the initial compressive wave travels through the skull from an outside source and reflects off of the opposite boundary of the skull. This reflection creates tensile wave that travels in the direction that the initial force came from and creates a low pressure region in the CSF for cavitation to exist [8]. There is little research that has been done on in vitro models of cavitation response, hence providing a compelling motivation for future studies [9].

1.2 Cavitation Creation and Methodology

Several approaches exist on experimentally studying the detriments that cavitation induces on nearby surfaces.

1.2.1 Propeller Rotation and Volumetric Flow Methods

Approaches seeking to characterize cavitation in propulsion and hydrodynamic pumping applications either use propellers, large pumps, or large engines to simulate this process, similar the Figure 1.1 [10]. In these methods the cavitation is chaotic and even the best imaging methods are challenged to fully characterize cavitation in real time. Flow meters and vacuum pumps are often used to initiate a cavitation environment in the flow.

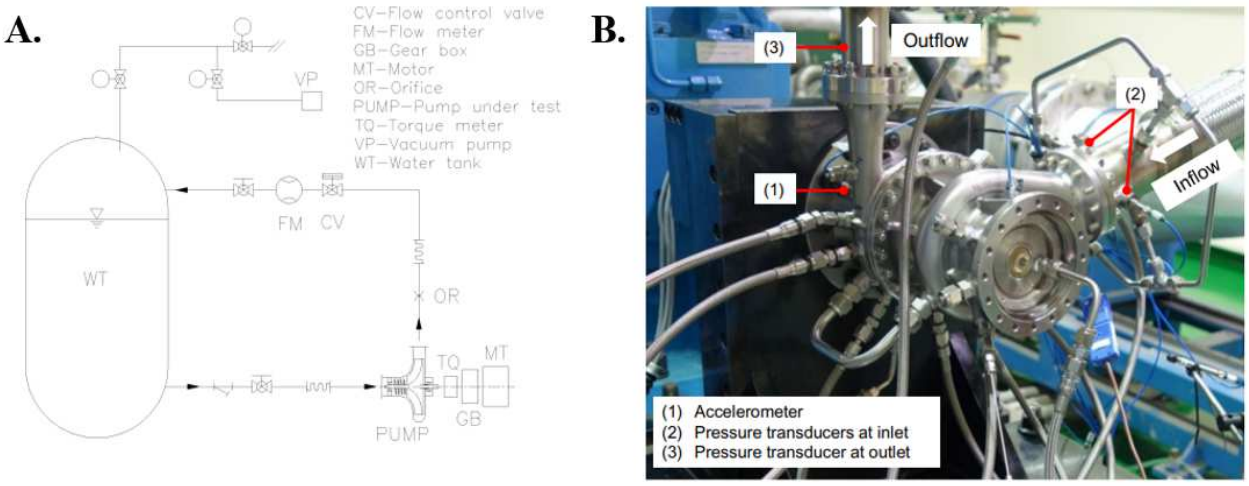

Figure 1.1: Cavitation apparatus schematic and illustration yielding chaotic cavitation in hydropump applications [10].

Cavitation erosion is often addressed in these applications by replacing the propeller or piping material with stainless steel or nickel aluminum bronze [11]. Anticavitation coatings are also used for existing materials in cavitation applications [1, 12]. For cavitation existing in the brain, applying an anticavitation coating is an impractical solution so different research and problem solving techniques have to be incorporated.

1.2.2 Controlled Cavitation Methods for Biomedical Applications

Sonoporation is known as the disruption of a membrane via ultrasound. This technique has been implemented in drug delivery applications by loading a MB with therapeutics and using acoustical cavitation to fragment and release the treatment once it has reached the desired location. The damage that this cavitation induces on surrounding cells has been studied using a dual-frequency transducer, shown in Figure 1.2.

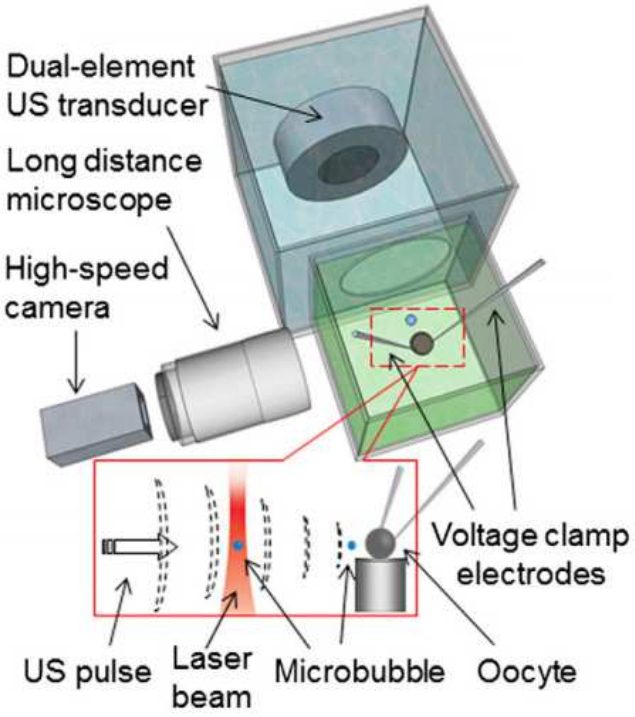

Figure 1.2: Controlled cavitation via optics, acoustics, and electrophysiological techniques [3].

MB generation is conducted using laser induced optical breakdown methods. After MB create they remained trapped and stable in the fs later beam. A dual-frequency transducer is used to position and collapse the MBs after they are isolated. The center transducer is used to help position and direct the MBs to target cells. After the MB position is optimized the outer (donut-shaped) transducer is used to induce resonant frequency conditions, which ultimately leads to

cavitation as the MB oscillates at maximum amplitude. A high speed camera is used in unison with a long distance microscope to visualize this phenomenon in real time. Voltage clamp electrodes are used to fix the spheroid cells of interest and monitor the transmembrane-current. This was ultimately a test to confirm cell viability throughout cavitation and ultrasound exposure [3]. This method offers a wide range of novelty in the realm of applied cavitation in biomedical applications. This technique is primarily advantageous at studying cavitation from a small number of MBs. This technique is also limited to laboratories that have access to the necessary optical, acoustical, and electrical components. Implementing this novel dual-frequency approach in a system that is able to produce arbitrary amounts of MBs would be advantageous for future cavitation studies.

Another cavitation creation approach involves designing an electrical circuit that generates shock wave bursts, resulting in the formation of MBs that collapse on nearby neuronal cells [13]. Figure 1.3 illustrates the specific electronic discharge apparatus that is implemented in this technique.

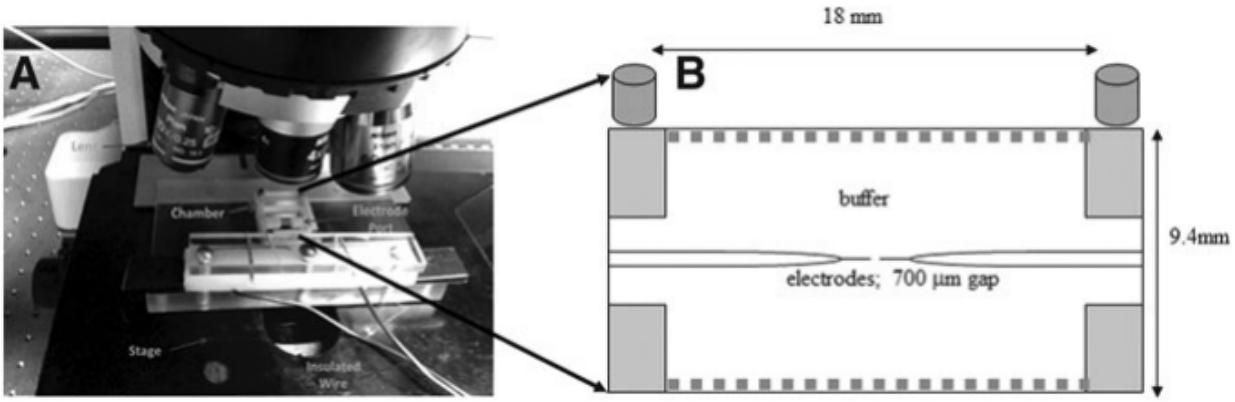

Figure 1.3: (A) Illustration of the complete analytic chamber mounted on the inverted microscope for live imaging. (B) A zoomed in schematic of the discharge chamber with neuronal cells seeded symmetrically above and below the electrodes [13].

As the two electrodes discharge they create MBs that rise and collapse on the surface of astrocytes seeded above. The astrocytes below the electrodes are used as a control, experiencing the shock wave from the electrical discharge but not experiencing exposure to cavitation. This is a novel apparatus that simulates cavitation damage on nearby brain cells. The biggest limiting factor in the application of this apparatus in future TBI studies is the limitation of produced MBs. Every discharge from the electrodes will produce a set range of MBs that rise to the surface. The presence of cavitation in the brain is confirmed in literature but the degree to which cavitation exists is still not fully characterized. Designing a system that allows for arbitrary amounts of MBs and cavitation exposure would yield additional novelty to this system.

1.3 Known Cellular/Tissue Response to Cavitation

The theory of cavitation being present in skull during a TBI is a modern theology. Because of this there is limited research characterizing cellular response to cavitation. Previous studies have looked at ovarian cells and found distinct pores left in the membrane because of nearby cavitation, illustrated in Figure 1.4 [3]. This is novel research and speaks to the damage that cavitation has on ovarian cells in therapeutic transport applications. Analyzing the damage from cavitation of a single MB also gives this study distinct novelty.

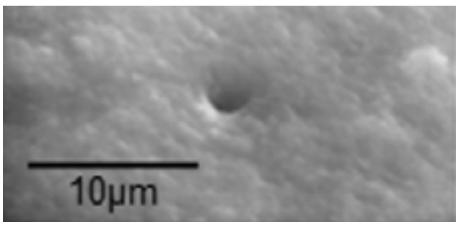

Figure 1.4: Cell membrane pore created from nearby cavitation of a single MB [3].

Other studies have analyzed the response that brain cells, more specifically astrocyte cells, undergo after experiencing cavitation from ~200 MBs [13]. Figure 1.5 summarizes the displacement of astrocytes after experiencing various amounts of cavitation exposure. In addition to cellular displacement this study also found that astrocytes exposed to cavitation produced increased levels of reactive oxygen species. These secretions are potentially detrimental to the cranial network, according to genetic studies conducted reactive astrocytes [14-16].

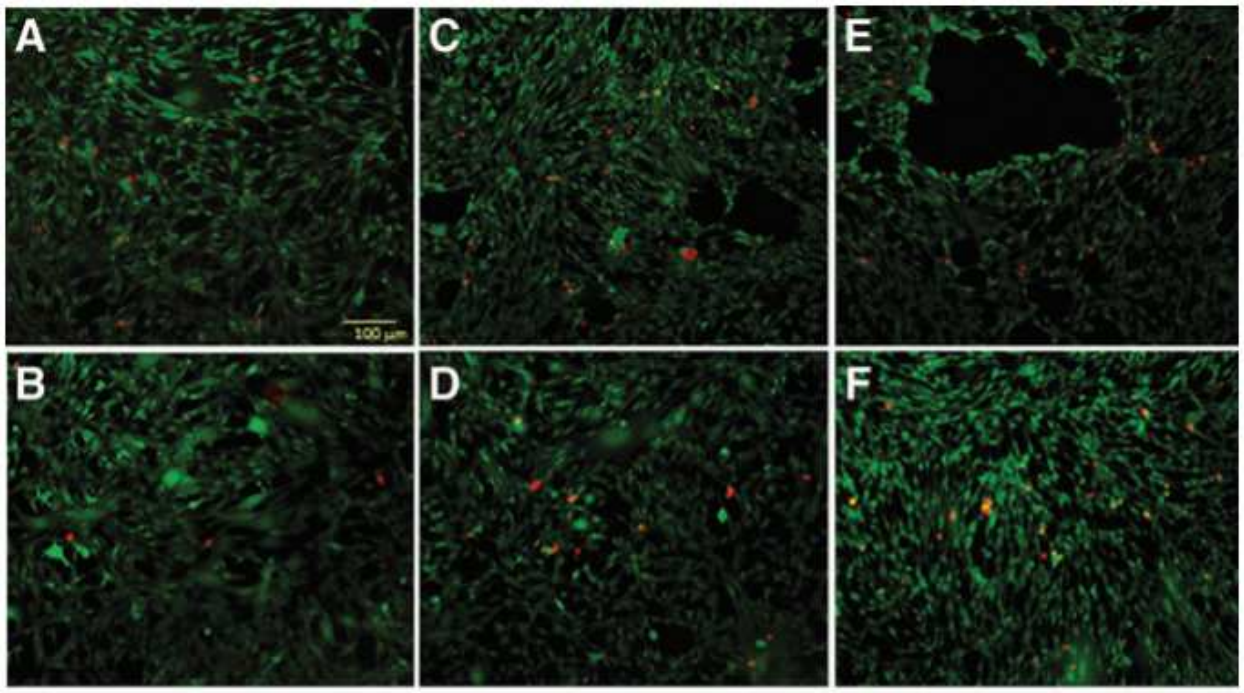

Figure 1.5: Frames A, C, E are experimental samples experiencing both the electronic shock wave and resulting cavitation. Frames B, D, F highlight the response that control astrocytes have after experiencing only shock wave exposure, not cavitation. The samples were exposed to one (A&B), three (C&D), and five (E&F) shock waves from the electronic circuit [13].

Additional studies have performed high strain environments on slices of the brain of a rat. Figure 1.6 summarizes the damage area of these trials. There are distinct changes that cavitation induces in this study but the scale of damage is likely different than that of what occurs *in vivo.* The size of the MBs in this study had a diameter larger than 1mm, significantly larger than what

likely happens *in vivo.* All in all, this study is novel by showing clear damage on cranial anatomy from cavitation. The damage is noticeable on the microscale for this amplified system. A future system that expands on this methodology but scales down the pressure magnitude and bubble size would add additional novelty.

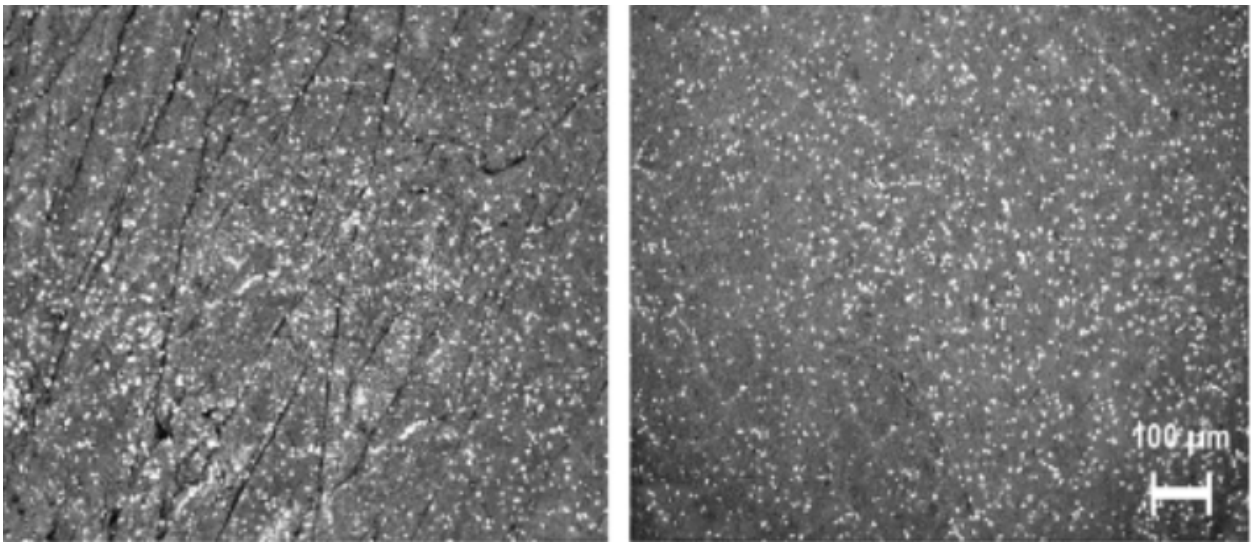

Figure 1.6: Microscale tears observed in slices of a rat brain due to cavitation exposure [9].

1.4 Motivation and Conclusion

Cavitation is known to exist in a wide variety of applications. Apparatus design considerations for studying cavitation effects in biomedical applications are significantly different compared to propulsion and hydropump applications. Due to the fact that cavitation existence in the skull during a TBI is a modern theory, there are limited studies on characterizing the response of cranial anatomy to this situation. Documented apparatus configurations that study this interaction introduce novel engineering that helps aid the knowledge of cavitation existence in the skull, but there are limitations and drawbacks to these methods as well. An apparatus that builds toward addressing these drawbacks is highlighted in chapter 2.

Studies have shown the cell membrane damage in ovarian cells, along with the cell displacement in astrocyte cells from cavitation. Additional studies have found distinct cavitation damage in various brain slices of a rat. These are novel studies that help raise awareness and motivation for further studies to investigate the response that neuronal cells undergo after exposure to cavitation. The force of cavitation has been consistently measured above the threshold pressures for brain damage to occur [5]. Because cavitation occurs for such a short duration, the significance of the damages that it induces on cranial anatomy is nearly entirely uncharacterized. Genetic and morphological changes of neuronal cells are sought to be investigated in the next chapters. These studies aim to further elucidate the nature of neuronal response to cavitation and help answer the various unknowns in this TBI realm.

References

[1] X. Qiao *et al.*, "Outstanding cavitation erosion resistance of hydrophobic polydimethylsiloxane-based polyurethane coatings," vol. 136, ed: Journal of Applied Polymer Science, 2019, p. 47668.

[2] D. Kang and K. Yokota, "Analytical Study of Cavitation Surge in a Hydraulic System," vol. 136, ed: Journal of Fluids Engineering-Transactions of the ASME, 2014, p. 101103.

[3] Y. Zhou, K. Yang, J. Cui, J. Y. Ye, and C. X. Deng, "Controlled permeation of cell membrane by single bubble acoustic cavitation," *Journal of Controlled Release,* vol. 157, no. 1, pp. 103-111, 2012.

[4] M. Wang, Y. Zhang, C. Cai, J. Tu, X. Guo, and D. Zhang, "Sonoporation-induced cell membrane permeabilization and cytoskeleton disassembly at varied acoustic and microbubble-cell parameters " vol. 8, ed: Scientific Reports, 2018, p. 3885.

[5] J. Goeller, A. Wardlaw, D. Treichler, J. O'Bruda, and G. Weiss, "Investigation of cavitation as a possible damage mechanism in blast-induced traumatic brain injury," vol. 29, ed: Journal of Neurotrauma, 2012, pp. 1970-1981.

[6] M. B. Panzer, B. S. Myers, B. P. Capehart, and C. R. Bass, "Development of a finite element model for blast brain injury and the effects of CSF cavitation," vol. 40, ed: Annals of Biomedical Engineering, 2012, pp. 1530-1544.

[7] A. Nakagawa *et al.*, "Shock wave-induced brain injury in rat: Novel traumatic brain injury animal model," vol. 102, ed: Acta Neurochirurgica Supplements, 2008, pp. 421-424.

[8] S. Haniff and P. A. Taylor, "In silico investigation of blast-induced intracranial fluid cavitation as it potentially leads to traumatic brain injury," vol. 27, ed: Shock Waves, 2017, pp. 929-945.

[9] S. Canchi, K. Kelly, Y. Hong, M. A. King, G. Subhash, and M. Sarntinoranont, "Controlled single bubble cavitation collapse results in jet-induced injury in brain tissue," vol. 74, ed: Journal of the Mechanical Behavior of Biomedical Materials, 2017, pp. 261-273.

[10] S. Hong and C. Choi, "Experimental Study on Cavitation Instabilities of Small Turbopump for Rocket Engine," vol. 60, ed: The Japan Society for Aeronautical and Space Sciences, 2017, pp. 230-234.

[11] H. Hiraga, T. Inoue, S. Hirofumi, and A. Matsumawa, "Cavitation erosion mechanism of NiTi coatings made by laser plasma hybrid spraying," vol. 231, ed: Wear, 1999, pp. 272-278.

[12] Y. Liu, Z. Hang, N. Xi, H. Chen, C. Ma, and X. Wu, "Erosion-Corrosion Behavior of HVOF WC-Co Coating in Cl− and SO42− Containing Solutions," vol. 431, ed: Applied Surface Science, 2018, pp. 55-59.

[13] S. Sun, J. Kanagaraj, L. Cho, D. Kang, S. Xiao, and M. Cho, "Characterization of Subcellular Responses Induced by Exposure of Microbubbles to Astrocytes," vol. 38, ed: Journal of Neurotrauma, 2015, pp. 1-8.

[14] S. A. Liddelow *et al.*, "Neurotoxic reactive astrocytes are induced by activated microglia," vol. 541, ed: Nature, 2017, pp. 481-487.

[15] S. A. Liddelow and B. A. Barres, "Reactive Astrocytes: Production, Function, and Therapeutic Potential," vol. 46, ed: Immunity, 2017, pp. 957-967.

[16] J. L. Zamanian *et al.*, "Genomic Analysis of Reactive Astrogliosis," vol. 32, ed: Journal of Neuroscience, 2012, pp. 6391-6410.

CHAPTER 2. CONTROLLED POSITIONING OF MICROBUBBLES AND INDUCED CAVITATION USING A DUAL-FREQUENCY TRANSDUCER AND MICROFIBER ADHESION TECHNIQUES

Modified from a manuscript published in Ultrasonics Sonochemistry

Alex H. Wrede[1], Aarthy Shah[1], Marilyn C. McNamara[1], Reza Montazami[1,2], and Nicole N. Hashemi[1,2]*

1 Department of Mechanical Engineering, Iowa State University, Ames, Iowa 50011, USA

2 Center for Advanced Host Defense Immunobiotics and Translational Comparative Medicine, Iowa State University, Ames, IA 50011, USA

Abstract

We report a study on two methods that enable spatial control and induced cavitation on targeted microbubbles (MBs). Cavitation is known to be present in many situations throughout nature. This phenomena has been proven to have the energy to erode alloys, like steel, in propellers and turbines. It is recently theorized that cavitation occurs inside the skull during a traumatic-brain injury (TBI) situation. Controlled cavitation methods could help better understand TBIs and explain how neurons respond at moments of trauma. Both of our approaches involve an ultrasonic transducer and bio-compatible polycaprolactone (PCL) microfibers. These methods are reproducible as well as affordable, providing more control and efficiency compared to previous techniques found in literature. We specifically model three-dimensional spatial control of individual MBs using a 1.6 MHz transducer. Using a 100 kHz

transducer, we also illustrate induced cavitation on an individual MB that is adhered to the surface of a PCL microfiber. The goal of future studies will involve characterization of neuronal response to cavitation and seek to unmask its linkage with TBIs.

2.1 Introduction

Cavitation refers to the spontaneous growth and collapse of MBs in low pressure regions. This process is currently used in a variety of areas, to mix fluids and eliminate impurities [1], as well as in specific drug delivery[2], gene therapy[3], and thrombolysis [4]. Previous research has also linked cavitation as a contributing factor in the exfoliation of graphene [5, 6]. Additionally, cavitation has been shown to produce shock waves that have erosive effects on objects such as turbines and propellers [7-9]. Cavitation has also shown to produce a wide range of bioeffects. Previous studies sought out to identify cell damage that occurs in the midst of ultrasound therapy via calcium signaling processes [10]. On top of this, interested parties suspect that cavitation occurs inside the skull of TBI victims and its aftermath is leaving a profound impact [11-14]. Generation and characterization of controlled cavitation is critical to understand the cellular mechanisms of TBIs. These understandings can lead to better treatment that improves the quality of life for TBI victims, or it can even help launch preventative techniques that reduce the chance of a TBI altogether. In this study we use capillary tubing and an ultrasonic transducer to create two cost-effective methods for controlled cavitation. Our expectation is that these methods will be advantageous and applicable in future studies that focus on studying and understanding on the effects that cavitation has on nearby surfaces, like neurons in a TBI situation.

Acoustic cavitation occurs when the instantaneous pressure is negative, and a process of nucleation takes place [15]**.** Upon collapse of these MBs, micro jets form, localizing impact and

force, causing damage to nearby surfaces[16]. This phenomenon is most visible in propellers, where the turbulent force of moving water creates areas of extreme low pressure, and over a period of time the blades experience significant erosion due to the repetitive impact of the cavitation shock waves [17]. There has been various techniques used in previous studies to study cavitation.

Acoustic, hydrodynamic, and optical methods have been implemented in previous studies to generate cavitation. In acoustic cavitation, ultrasonic waves are used to create cavitation, however previous methods do not have arbitrary control in the quantity of produced MBs and the specific location of their collapse is variant [18]. In hydrodynamic cavitation, fluid flows through an orifice, which increases the velocity and subsequently lowers threshold pressure so that nucleation occurs at the point of entry. With this method, vast amounts of MBs are generated, preventing the ability to analyze the effects of finite cavitation [19]. In optical induced cavitation, an intense energy is introduced to the system (laser), creating a stream of MBs in the beam of the laser. While this method is practical in creating controlled amounts of MBs, lasers are expensive and not accessible for a lot of research groups. Our approach is economical and offers a modification to the acoustic method to ultimately create a controlled environment to observe the effects of cavitation.

We introduced MBs into a water tank at a controlled size by pushing air through capillary tubing. We implemented two separate techniques to arbitrarily trap and position the MBs before induced cavitation. Our first method involves the use of a dual-frequency transducer [20]. The second method involves the MBs adhering to the surface of finely positioned PCL microfibers as they rise in solution. Using these techniques we were able to create, position, and collapse a finite number of MBs, as well as successfully illustrate live cavitation. These approaches are

reproducible as well as affordable, providing more controlled and efficient techniques for cavitation studies.

2.2 Materials and Methods

2.2.1 MB Production

Capillary tubing with an inner diameter of 5 μm and an outer diameter of 360 μm (Molex, Lisle, IL), was used to produce the MBs. The tubing was attached to a 3 mL luer-lock syringe filled with air using a tubing adapter (Idex, Lake Forest, IL). A syringe pump (GenieTouch, Kent Scientific, Austin, TX) was used to plunge the syringe at a constant rate, allowing for the constant release of consistent sized MBs. The accuracy of all measurements were within ~2.7 μm due to the resolution of our imaging techniques. Sections 2.2.2 and 2.2.3 overview controlled cavitation via the dual-frequency method and via adhesion and resonant frequency, respectively. This orientation is followed throughout the Materials and Methods, Results, and Discussion sections.

2.2.2 Controlled MB Positioning Through a Dual-frequency Transducer

Figure 2.1A represents the experimental setup for controlled MB positioning through the incorporation of a dual-frequency transducer. A 1.5 gallon tank filled with deionized water was used to house the existing components. This method was established through a developed study [20] which involves a point-focused, donut-shaped, (inner diameter of 14 mm and outer diameter of 30 mm, focal distance of 48mm) ultrasound transducer with a center frequency of 1.6 MHz (ndtXducer, LLC, Northborough, MA). The transducer emitted brief ultrasound pulses to trap the MBs at the focus without collapsing them. The dual-frequency transducer is suspended in mid-

solution through the attachment with a 3-axis adjustable stage (MT1, Thor Labs, Newton, New Jersey). This stage allows 3D arbitrary movement of the transducers, which ultimately leads to 3D spatial control over MBs after they are trapped. PCL microfibers (Hashemi Lab, Iowa State University, Ames, IA) were placed above the capillary tubing and at the focal point of the transducer. There are three main reasons that the PCL microfibers were chosen to be used for this method. First, they have a delicate nature[21], allowing minimal disruption to the MBs and pressure field induced by the transducer upon entrapment. Second, they are used as a point of reference during the characterization of MB positioning. Lastly, these microfibers are known for their biocompatibility and potential in many future studies[22]. When not in simulation, the microfibers were preserved in ethanol to prevent infection and swelling. With the transducer focused at the level of the PCL microfibers and in line with the rising MBs, we were able to consistently trap and isolate individual MBs next to the PCL microfibers.

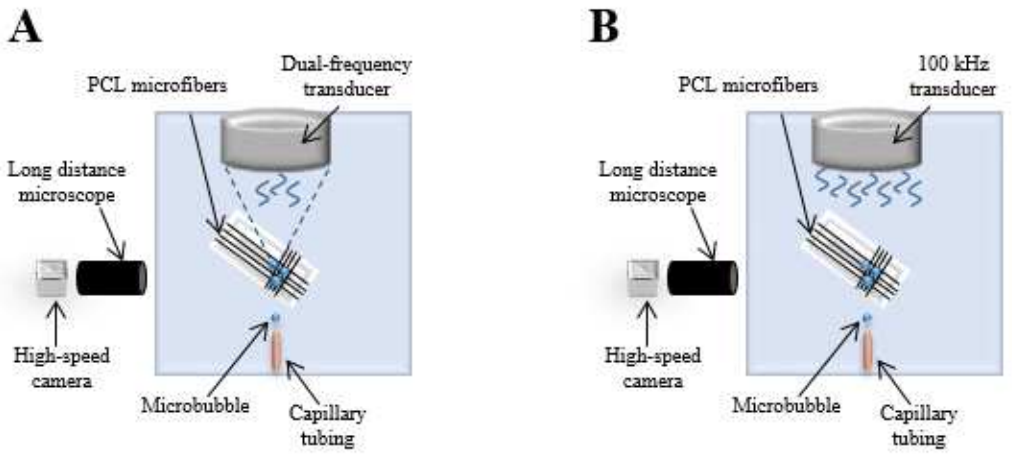

Figure 2.1: (A) Apparatus for controlled MB positioning and collapse through using a dual-frequency transducer. The gap between the tip of the capillary tubing and the ultrasonic transducer was 70mm. The gap between the PCL fibers and the ultrasonic transducer is 48mm. The MBs are trapped at the focus of the 1.6 MHz outer-transducer (lowermost tip of the dotted lines). The 100 kHz central transducer is unfocused and is emitting sinusoidal waves. (B) Apparatus of controlled MB positioning and cavitation through adhesion and resonant frequency. The gap between the tip of the capillary tubing and the ultrasonic transducer is 70mm. The gap between the PCL fibers and the transducer is 22.5mm.

The central transducer induces oscillation on the MBs which ultimately leads to their collapse. The resonant frequency of a MB refers to the frequency at which it oscillates at a relative maximum amplitude[23]. When a MB oscillates with enough magnitude, it begins to fragment into smaller MBs, creating cavitation[24]. Equation 1 represents the necessary calculation to find the resonant frequency of a MB with a known radius:

$$f_0 = 2\pi \sqrt{\frac{3\gamma P_0 + \frac{2\sigma}{R_0} - \frac{2\sigma}{R_0}}{\rho R_0^2}} \quad (1)$$

In this calculation, f_0 represents the first resonant frequency, R_0 designates the nominal bubble radius, ρ is the suspending mass density, γ denotes the gas phase polytropic constant, P_0 is the ambient pressure, and σ symbolizes the surface tension [25]. The size of the MBs generated through the capillary tubing ranged from 50-100 µm in diameter throughout our study. Plugging in the necessary parameters for Equation 1, a MB with a 60 µm diameter will oscillate at a resonant frequency of ~100 kHz. We decided to use a 100 kHz transducer (diameter of 45mm, unfocused) (Olympus, Waltham, MA) to achieve dramatic oscillation near the resonant frequency for 50-100 µm MBs. Since prior studies have shown the effectiveness of simultaneous dual-frequency functionality [20], it was ignored in this study. Our motivation is to demonstrate that a dual-frequency transducer would be effective through the combination of our positioning and cavitation results. The transducers were driven by a power amplifier (RAM-5000, Ritec, Warwick, RI). The magnified high-speed analysis was achieved by using a long distance microscope (Model K2, Infinity Photo-Optical Company) in unison with a high speed camera for imaging (BlackFly, FLIR).

2.2.3 Controlled MB Positioning and Collapse Through Adhesion and Resonant Frequency

The second method of controlled MB positioning and collapse is represented in Figure 2.1B. PCL microfibers are also used in this approach and they are advantageous due to their ability to be adhesive to rising air bubbles. As the rising MBs came in contact with the PCL microfibers, they adhered to its surface. The PCL microfiber scaffold is suspended in mid-solution through the attachment with a 3-axis adjustable stage (MT1, Thor Labs, Newton, New Jersey). Three-dimensional control over the position of the scaffold allows for arbitrary control over the magnitude and position of trapped MBs. The transducer used in this approach is primarily to induce cavitation and has no influence on trapping and positioning of MBs. A 100 kHz transducer is also used in this method to accommodate resonant frequency conditions. The 100 kHz transducer is placed 22.5mm (1/2 transducer diameter) above the PCL microfibers to maximize oscillation. The ultrasonic transducer was driven by a power amplifier (RAM-5000, Ritec, Warwick, RI). The high-speed analysis was achieved by using a long distance microscope (Model K2, Infinity Photo-Optical Company) in unison with a high speed camera for imaging (BlackFly, FLIR).

2.3 Results

2.3.1 MBs Released from Capillary Tubing

Using different flow rates on the syringe pump, different sized bubbles can be generated. The rate at which MBs exit the capillary tubing can also vary. Figure 2.2A shows MBs releasing from the capillary tubing at ~50 μm in diameter. This particular trial was operating with a flow

rate of 100 µL/min on the syringe pump and they released from the capillary tubing at a rate of 50 MB/min. As the MBs increased in size, they required a greater pressure to collapse them. To create a greater pressure, the amplification of voltage to the transducer must also increase. Figure 2.2B represents the necessary peak-to-peak voltage to fragment MBs with varying sizes. In other words, 100 kHz is approximately the resonant frequency of a 60 µm MB but it can induce cavitation on similar sized MBs if the operating voltage is varied. Varying the operating voltage also varies the acoustical pressure that is induced on the MBs.

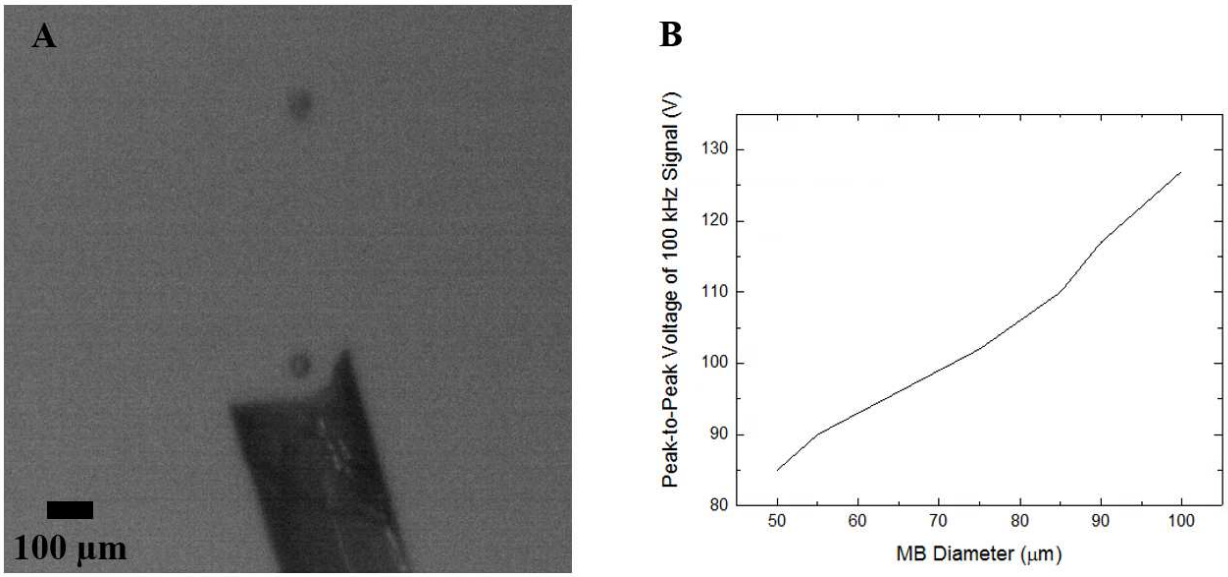

Figure 2.2: (A) Air MBs releasing from capillary tubing. (B) Relationship between MB diameter and corresponding peak-to-peak voltage through the 100 kHz transducer that is necessary to collapse bubbles.

2.3.2 MB Positioning Using Dual-frequency Method

Previous studies have shown that the impact of cavitation is most significant when the space between the MB and target material (D) is less than the diameter of the MB (d). The cavitation effects are greatly reduced when this ratio (D/d) increases [20]. Figure 2.3 demonstrates the ability of the point-focused transducer to trap and suspend a MB in mid-

solution through a pulsed signal (central frequency 1.6 MHz, 20 cycles, pulse repetition frequency 238 Hz, 250Vpp). Arbitrarily adjusting the 3-axis stage allowed for MB positioning toward the PCL microfiber. The MBs in Figure 2.3 are moving at approximately 30 µm/sec until they are held stationary when D<d. This was a typical speed for our trials because the MBs would often escape the focal region of the transducer if the adjustable stage was moved at a faster rate.

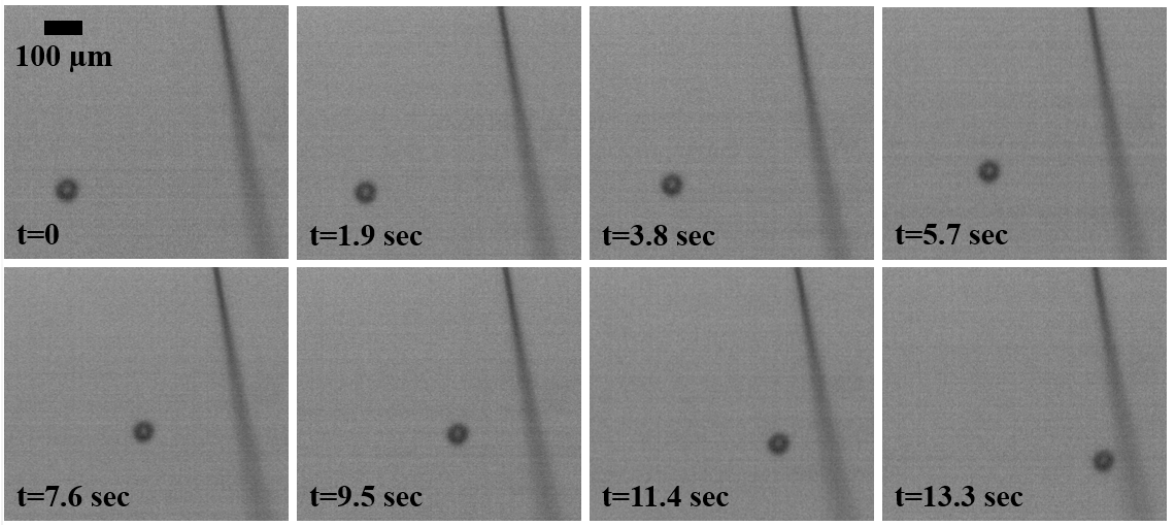

Figure 2.3: Lateral MB positioning using the 1.6 MHz point-focused transducer.

After the MBs were directed D<d away from the target material, our apparatus also had arbitrary control over the vertical depth that the MBs resided in mid-solution. Figure 2.4 shows the vertical dimension of the MB being adjusted as it remains D<d away from the PCL microfiber (central frequency 1.6 MHz, 20 cycles, pulse repetition frequency 238 Hz, 250 Vpp). The MBs are less resistive to ascent in solution compared to movement in any other direction because of their buoyancy. The MBs represent this tendency in Figure 2.4 as they rise around 75 µm/sec.

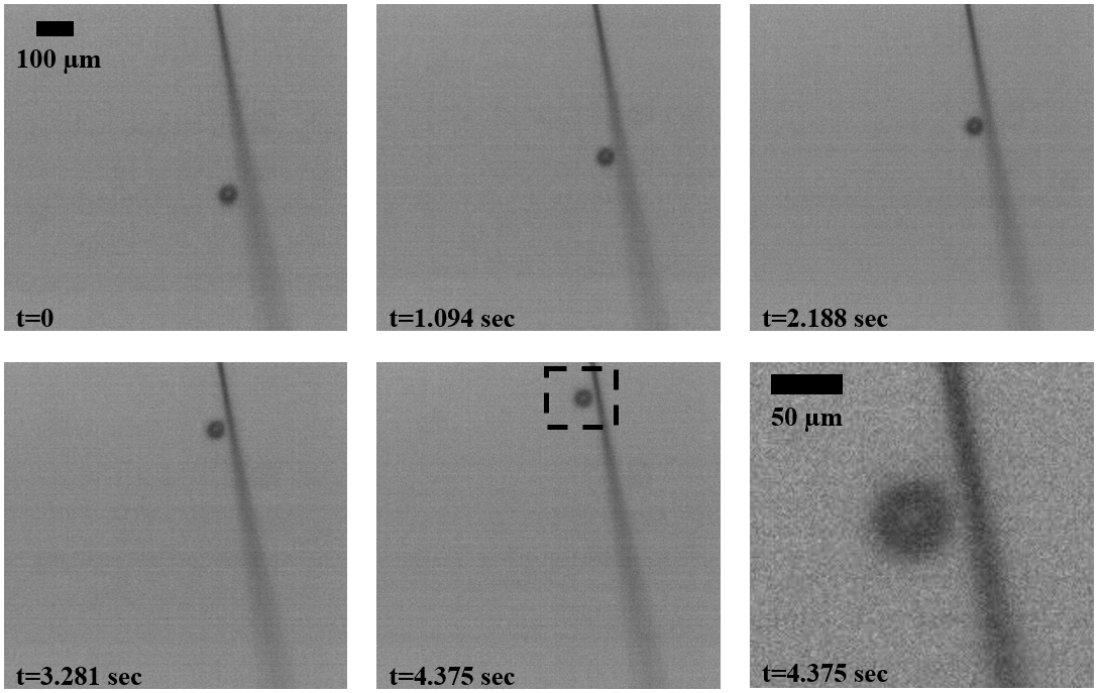

Figure 2.4: Vertical MB positioning using the 1.6 MHz point-focused transducer. The final image is zoomed upon to show that the MB is clearly within one MB diameter length (D) from the PCL microfiber. It is estimated that at 4.375 seconds, the distance between the MB and the PCL microfiber is ~8 µm.

2.3.3 MB Positioning and Collapse Using Microfiber Adhesion and Resonant Frequency

Having complete control over the position of the PCL microfiber scaffold allowed for arbitrary control over the magnitude and position of trapped MBs. The scaffold is placed directly above the path of rising MBs and "catches" any MBs that come in contact with the PCL microfiber surface. After the MBs are trapped at desired locations, the scaffold is moved away from the rising MBs to eliminate any disturbance on the controlled environment. The 100 kHz transducer is then centered above the scaffold and used to induce cavitation (4 cycles, pulse repetition frequency 59 Hz, 100 Vpp). Figure 2.5 captures this phenomena at high speed. After 16 ms the original MB is shown to fragment into three smaller MBs, illustrating cavitation.

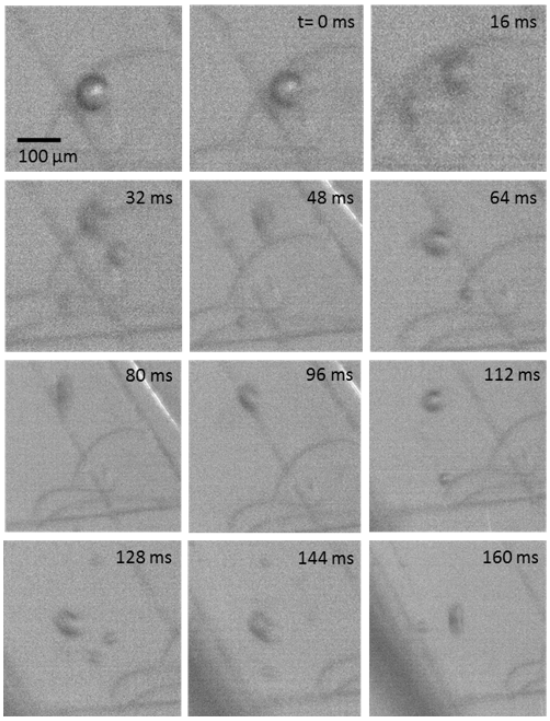

Figure 2.5: Induced cavitation from the resonant frequency that the 100 kHz transducer provides. The images are captured at 62 f/sec.

2.4 Discussion

Although it is suspected that MBs form and collapse to create cavitation inside the skull during TBI situations [11], there is no direct research to understand the neuronal response to this phenomena. This research could be the underlying building block that is used to answer questions about the nature of TBIs and the symptoms that they endow. Generating controlled cavitation is the first step to simulating these responses. Previous methods for the creation of cavitation are uncontrolled, and/or uneconomical. In this study, we developed a novel approach combining microfluidic and acoustical methods to create economical controlled cavitation. This approach offers intriguing potential for future studies to analyze the effects that cavitation has on surrounding materials. The PCL microfibers used in this study have been shown to successfully

sustain living cells in previous research[22], which provides direct opportunity for bio-medical applications in future research.

2.4.1 MB Production

We were able to generate MBs at a consistent rate, with the size of 50-100 μm. The generated MBs released from the tubing at a constant size throughout each trial but a given set of experimental parameters did not always produce the same size MBs from one trial to the next. This was not critical, though, because the size of the MBs remained within 50-100 μm, the range at which we hoped to produce for applications previously listed. Also, for our study it was more important to get constant release of MBs with similar sizes than to have a narrow tolerance on the size variance from one trial to the next. A possible reason for the variability in size might be due to the erosion on the capillary tubing inside the luer-lock adapter. The pressure built up at this point is immense due to the difference in cross sectional area between the syringe and capillary tubing. We would occasionally recut the tubing to get rid of eroded material but the difference from one cut to the next is difficult to replicate on tubing with a 5 μm inner diameter and an outer diameter of 360 μm. A difference in the pattern of this cut likely changes the airflow inside the tubing and could be the underlying reason for variability in MB size. The rate at which the MBs exited the capillary tubing was also variant, likely due to similar reasons. This was not a critical issue in our study, as the 1.6 MHz was able to trap and isolate individual MBs regardless of their repetition rate. The rate at which they exited was also at a slow enough rate to "catch" arbitrary amounts of MBs with the PCL microfibers.

Using air as the gas that make up the MBs is advantageous when applying our project to a TBI situation. During a blast-induced TBI, MBs are expected to form inside the extracellular

matrix which is concentrated with cerebrospinal fluid (CSF) that is primarily made up of water vapor, oxygen, and nitrogen [26]. Due to the similar chemical makeup of air, we decided its substitution in this project to realistically resemble a cavitation bubble from a blast-induced TBI is reliable.

2.4.2 MB Positioning Using Dual-frequency Method

An acoustical method for MB positioning was used in previous studies, which incorporated a dual-frequency transducer [20]. We extended on this approach by making future studies more advantageous for TBI studies. Previous research used optical methods to produce MBs which is often times uneconomical. We combined our MB production method (Section 2.2.1) with their acoustical methods to demonstrate 3D control over cavitation in a more economical manner. Using microfibers in our apparatus also allows for the study of a wide variety of cells in future studies. Previous methods have used voltage clamp electrodes to constrain cells but this is not feasible to maintain cell-viability for all types of cells. Our methods are advantageous to produce and have 3D control over MBs that are 50-100 μm, but if future works requires smaller MB size (~10 μm) then optical methods, similar to that of Zhou et al., would be more advantageous.

We ignored simultaneous positioning and cavitation through dual-frequency capability in this study but our combined results (Sections 2.3.2 & 2.3.3) demonstrate that a dual-frequency transducer with an outer frequency of 1.6 MHz and a central frequency of 100 kHz would be successful in doing so for future studies. This proven functionality provides direct opportunity to study the controlled effects that cavitation has on surrounding materials. Having the ability to

arbitrarily control the spatial displacement between the MBs and target material (D) also provides opportunity to study the relationship between D and the target material response.

2.4.3 MB Positioning and Collapse Using Microfiber Adhesion and Resonant Frequency

The methods and results shown in Sections 2.2.3 & 2.3.3 demonstrate encouraging capability that has potential to propel future studies. Due to the delicate nature of the PCL microfibers [27], future studies on cavitation characterization can be done. Our novel approach allows for the MBs to be trapped as they adhere to the surface of the microfibers. As cavitation occurs, the microfibers will have minimal disruption on its pattern, allowing for a detailed analysis on the stages of cavitation and its aftermath. The biocompatibility of the PCL microfibers will allow for the introduction of cell-laden microfibers[22], and ultimately will provide opportunity for future research on the effects of surface-cavitation and its consequences on surrounding cells. In regards to a TBI situation, using neuron-laden microfibers in our apparatus offers a realistic model that will mimic the consequences that surface-cavitation has on surrounding neurons. 3D control over the scaffold will allow for MB positioning and cavitation on arbitrary neurons.

2.5 Conclusions

In this study we have shown the success of MB production with a corresponding size of 50-100 μm. We have also demonstrated the success of two methods of controlled cavitation. . These methods are cost-effective and provide arbitrary control on the position and magnitude of cavitation. These methods provide intriguing potential for future studies focused on the effects of cavitation on variable surfaces. In response to TBIs specifically, the two methods of controlled

cavitation presented in this study provide an excellent opportunity to gather a detailed study on the neuronal response to cavitation. Future research that builds off of the techniques in this study involves using the biocompatibility of the PCL microfibers to seed neurons on its surface [22]. Using these neuron-laden microfibers in both of these methods will allow for characterization of neuronal response to cavitation and seek to unmask the unanswered questions in TBIs.

References

[1] P. R. Gogate and A. M. Kabadi, "A review of applications of cavitation in biochemical engineering/biotechnology," vol. 44, ed: Biochemical Engineering Journal, 2009, pp. 60-72.

[2] C. M. Schoellhammer and G. Traverso, "Low-frequency ultrasound for drug delivery in the gastrointestinal tract," vol. 13, ed: Expert Opinion on Drug Delivery, 2016, pp. 1045-1048.

[3] C. M. H. Newman and T. Bettinger, "Gene therapy progress and prospects: Ultrasound for gene transfer," vol. 14, ed: Gene Therapy, 2007, pp. 465-475.

[4] E. P. Stride and C. C. Coussios, "Cavitation and contrast: the use of bubbles in ultrasound imaging and therapy," in *Institution of Mechanical Engineering*, 2009, vol. 224, no. 2, pp. 171-191.

[5] Y. Gai, W. Wang, D. Xiao, and Z. Yaping, "Ultrasound coupled with supercritical carbon dioxide for exfoliation of graphene: Simulation and experiment," vol. 41, ed: Ultrasonics Sonochemistry, 2018, pp. 181-188.

[6] R. K. L. Tan *et al.*, "Graphene as a flexible electrode: review of fabrication approaches," vol. 5 ed: Journal of Materials Chemistry A, 2017, pp. 17777-17803.

[7] A. Philipp and W. Lauterborn, "Cavitation erosion by single laser-produced bubbles," vol. 361, ed: Journal of Fluid Mechanics, 1998, pp. 75-116.

[8] L. Chernin and D. V. Val, "Probabilistic prediction of cavitation on rotor blades of tidal stream turbines," vol. 113, ed: Renewable Energy, 2017, pp. 688-696.

[9] J. Bin, L. Xianwu, and Y. Wu, "Unsteady cavitation characteristics and alleviation of pressure fluctuations around marine propellers with different skew angles," vol. 28, ed: Journal of Mechanical Science and Technology, 2014, pp. 1339-1348.

[10] F. Li *et al.*, "Dynamics and mechanisms of intracellular calcium waves elicited by tandem bubble-induced jetting flow," ed: PNAS, 2017.

[11] J. Goeller, A. Wardlaw, D. Treichler, J. O'Bruba, and G. Weiss, "Investigation of Cavitation as a Possible Damage Mechanism in Blast-Induced Traumatic Brain Injury," vol. 29, ed: Journal of Neurotrauma, 2012, pp. 1970-1981.

[12] S. Canchi, K. Kelly, Y. Hong, M. A. King, G. Subhash, and M. Sarntinoranont, "Controlled single bubble cavitation collapse results in jet-induced injury in brain tissue," vol. 74, ed: Journal of the Mechanical Behavior of Biomedical Materials, 2017, pp. 261-273.

[13] R. S. Salzar, D. Treichler, A. Wardlaw, G. Weiss, and J. Goeller, "Experimental Investigation of Cavitation as a Possible Damage Mechanism in Blast-Induced Traumatic Brain Injury in Post-Mortem Human Subject Heads," vol. 34, ed: Journal of Neurotrauma, 2017, pp. 1589-1602.

[14] C. M. Cartagena *et al.*, "Subacute Changes in Cleavage Processing of Amyloid Precursor Protein and Tau following Penetrating Traumatic Brain Injury," vol. 11, ed: PLOS ONE, 2016.

[15] C. E. Brennen, *Cavitation and Bubble Dynamics*. Cambridge: Cambridge University Press, 2013.

[16] W. Lauterborn and C.-D. Ohl, "Cavitation bubble dynamics," *Ultrasonics Sonochemistry,* vol. 4, no. 2, pp. 65-75, 1997.

[17] G. Kuiper, "Cavitation Research and Ship Propeller Design," *Applied Scientific Research,* vol. 58, pp. 33-50, 1998.

[18] M. Ashokkumar, "The characterization of acoustic cavitation bubbles – An overview," *Ultrasonics Sonochemistry,* vol. 18, no. 4, pp. 864-872, 2011.

[19] P. R. Gogate and A. B. Pandit, "A review and assessment of hydrodynamic cavitation as a technology for the future," *Ultrasonics Sonochemistry,* vol. 12, no. 1, pp. 21-27, 2005/01/01/ 2005.

[20] Y. Zhou, K. Yang, J. Cui, J. Y. Ye, and C. X. Deng, "Controlled permeation of cell membrane by single bubble acoustic cavitation," *Journal of Controlled Release,* vol. 157, no. 1, pp. 103-111, 2012.

[21] Z. Bai, J. M. M. Reyes, R. Montazami, and N. Hashemi, "On-chip development of hydrogel microfibers from round to square/ribbon shape," vol. 2, ed: Journal of Material Chemistry A, 2014, pp. 4878-4884.

[22] F. Sharifi, B. B. Patel, A. K. Dzuilko, R. Montazami, D. S. Sakaguchi, and N. Hashemi, "Polycaprolactone Microfibrous Scaffolds to Navigate Neural Stem Cells," *Biomacromolecules,* vol. 17, pp. 3287-3297, 2016, doi: 10.1021/acs.biomac.6b01028.

[23] D. B. Khismatullin, "Resonance frequency of microbubbles: Effect of viscosity," vol. 116, ed: Journal of Acoustical Society of America, 2004, pp. 1463-1473.

[24] M. Postema, A. Van Wamel, C. Lancee, and N. De Jong, "Ultrasound-induced encapsulated microbubble phenomena," vol. 30, ed: Ultrasound in Medicine and Biology, 2004, pp. 827-840.

[25] J. C. Buckey, D. A. Knaus, D. L. Alvarenga, M. A. Kenton, and P. J. Magari, "Dual-frequency ultrasound for detecting and sizing bubbles," *Acta Astronautica,* vol. 56, no. 9, pp. 1041-1047, 2005.

[26] S. Haniff and P. A. Taylor, "In silico investigation of blast-induced intracranial fluid cavitation as it potentially leads to traumatic brain injury," vol. 27, ed: Shock Waves, 2017, pp. 929-945.

[27] F. Sharifi, B. Patel, A. Dzuilko, R. Montazami, D. S. Sakaguchi, and N. Hashemi, "Polycaprolactone Microfibrous Scaffolds to Navigate Neural Stem Cells," vol. 17, ed: Biomacromolecules, 2016, pp. 3287-3297.

CHAPTER 3. SEEKING INSIGHT ON TBIS BY ANALYZING CAVITATION-INDUCED DAMAGE OF SOFT POLYMER FILMS

Modified from a manuscript submitted in Ultrasonics Sonochemistry

Alex H. Wrede[1], Faisal Al-Masri[1], Reza Montazami[1], and Nicole N. Hashemi[1,2]*

[1] Department of Mechanical Engineering, Iowa State University, Ames, Iowa 50011, USA

[2] Department of Biomedical Sciences, Iowa State University, Ames, IA 50011, USA

Abstract

Traumatic brain injuries (TBIs) are complex phenomena that create epidemic healthcare and financial concerns. Recent studies have theorized that cavitation exists during a TBI, which has potential to induce significant damages to surrounding anatomy. This study seeks to implement polydimethylsiloxane (PDMS) films as a placeholder of the brain to elucidate the damage that surrounding brain tissue would experience from nearby cavitation. The apparatus includes an existing methodology that implements controlled cavitation. 3D confocal microscopy and interferometry techniques are used to characterize the surface damage on the PDMS films. Visual representation and roughness parameters on the nanoscale help elucidate a distinct difference between control and experimental samples. These results help legitimize the concern of cavitation in the skull and also help motivate future studies to analysis the cellular response to surrounding cavitation.

3.1 Introduction

Despite decades of research, the brain continues to be one of the most obscure parts of the human body. TBI is the damaging aftermath to the brain due to a mechanical force, leading to functionality impairment. Exposure to blasts has led to a TBI in over 60% of soldiers serving in Iraq and Afghanistan[1]. Everyone in society is susceptible to a TBI, this diagnosis is typical in falls and automobile collisions. TBIs are also prevalent in contact sports where athletes are often exposed to cranial impacts[2]. There are many different leading causes and brain response mechanisms to TBI damage[3, 4]. Recent studies suggest the presence of cavitation in the human skull as a results of a TBI, which can arise due to the presence of small pockets of vapor in the cerebral spinal fluid (CSF) [5-7]. Upon impact these vapor contents expand and collapse due to a low pressure wave that reflects off the skull boundary after the initial compressive wave travels through the skull[8]. Cavitation has been proven to lead to significant erosion in alloys and hard plastics, applying a force that has been broadly characterized to a broad magnitude of 0.1-20 MPa [9-13]. If cavitation has the ability to erode steel, its potential to cause damage to much softer brain tissue is alarming.

In this study, we investigate the topographical changes that cavitation induces to PDMS films to help illustrate the damage that cavitation has on brain tissue. Soft materials have been consistently used to model organs in vitro as well as in tissue engineering[14]. Soft polymers have been a common candidate for this as they are easy and affordable to manufacture, and their elastic properties can be easily altered and studied[15]. Adjusting the base to curing agent ratio in the PDMS fabrication process allows for arbitrary selection to the mechanical properties of the PDMS.

The apparatus used to create cavitation on the PDMS films is similar to that used in previous studies[16]. This method is advantageous because it allows for controlled cavitation, enabling similar cavitation exposure from one sample to the next. Characterization of cavitation aftermath is characterized using 3D confocal microscopy and interferometry methods. This analysis yields novelty in multiple research disciplines, like propulsion and hydrodynamic pumping, but in the TBI realm it helps unmask the physical detriments that cavitation has on nearby neuronal anatomy. Understanding this aftermath is a vital piece to advance TBI recovery, prevention, and care.

3.2 Materials and Methods

3.2.1 PDMS Fabrication & Cavitation Apparatus

The PDMS samples were made by mixing the base and curing agent (Sylgard 184, Dow Corning, Midland, MI) at a 32:1 ratio and allowing them to cure at room temperature for 48 hours. Controlling the mass ratio of base to curing agent affects the hardness of the PDMS with higher ratios producing softer PDMS. The hardness of the PDMS samples are ~50 shore (PHT-960, Phase II, Upper Saddle River, NJ), which is slightly harder than that of the human brain which has been measured at 10-30 shore in previous studies[1]. Each PDMS sample was collect and cured in a petri dish with a diameter of 36 mm.

The complete apparatus configuration was followed closely to the adhesion technique outlined in previous studies[16]. The PDMS-filled petri dishes were suspended mid-solution using a 3-axis stage, and oriented in line of the stream of rising microbubbles (MBs). MBs exited the capillary tubing at a rate of ~75 MB/min. For each trial 450-500 MBs were collected across the exposed PDMS surface. After MB collection the sample was displaced out of plane with the

rising MBs and rotated 180° so it was exposed to a ultrasonic transducer, similar to the orientation in previous research[16]. The activation of the transducer creates resonant conditions for the collected MBs and ultimately induces cavitation (100 kHz center frequency, 5 cycles, pulse repetition frequency 59 Hz, 260 Vpp). The process of collecting MBs, rotating the PDMS substrate, and inducing cavitation was done ten times for each sample. Control samples were submerged in the tank and exposed to the transducer signal but they did not have any adhered MBs, eliminating the occurrence of cavitation. The control samples experienced ultrasound exposure to ensure that any observed topographical differences were solely due to cavitation forces.

3.2.2 Topography Analytics

The topographical analysis was conducted using 3D confocal microscopy and interferometry techniques (S neox, Sensofar, Barcelona, Spain). The compatible software (SensoSCAN v6.3) calculates roughness parameters that provide detailed characteristics of the sample topography. These parameters are useful when deciphering the difference between surface impurities, noise, and cavitation damage. All 3D confocal microscopy trials were conducted using a 150X objective lens, red light, and 60% lighting. Interferometry methods implement a 50XDi objective lens, green light, and 15% lighting. Both of these methods are used to legitimize topographical summaries of the PDMS surfaces on the nanoscale.

3.3 Results and Discussion

3.3.1 3D Confocal Microscopy

The 3D confocal microscopy system has an assortment of capabilities and objective options. Figure 3.1 represents a typical illustration of the surface of a control sample. Using a 150X objective lens condenses the dimensions of the field of view significantly. A stitched 3X3 field scan is implemented to collect data across a larger area and eliminate any bias from one particular region. Figure 3.2 illustrates the typical topography of an experimental sample after experiencing surrounding cavitation. A visual comparison yields distinct differences in the nature of the surface between the two samples. It appears that the cavitation has a created wear and erosion-like effects as small tears are visible on the surface of the PDMS. These damages are consistently visually present in the experimental samples and absent in the control samples. The damage from cavitation is further elucidated through roughness parameters that are internally calculated in the software. The roughness parameter '*Sa*' is used to portray the overall roughness of the surface by calculating the magnitude of the difference in height from the mean height. The *Sa* calculation gives an optimal description of the surface roughness due to the fact that in the derivation, impurities or foreign objects adhered to the surface have a minimal effect on the final value[17]. The average *Sa* value for all the control surfaces was calculated at 22.0 nm. This value is noticeably different than the experimental samples, which had an average *Sa* value of 28.8 nm. This increase in roughness is expected due to the cavitation damage that is introduced.

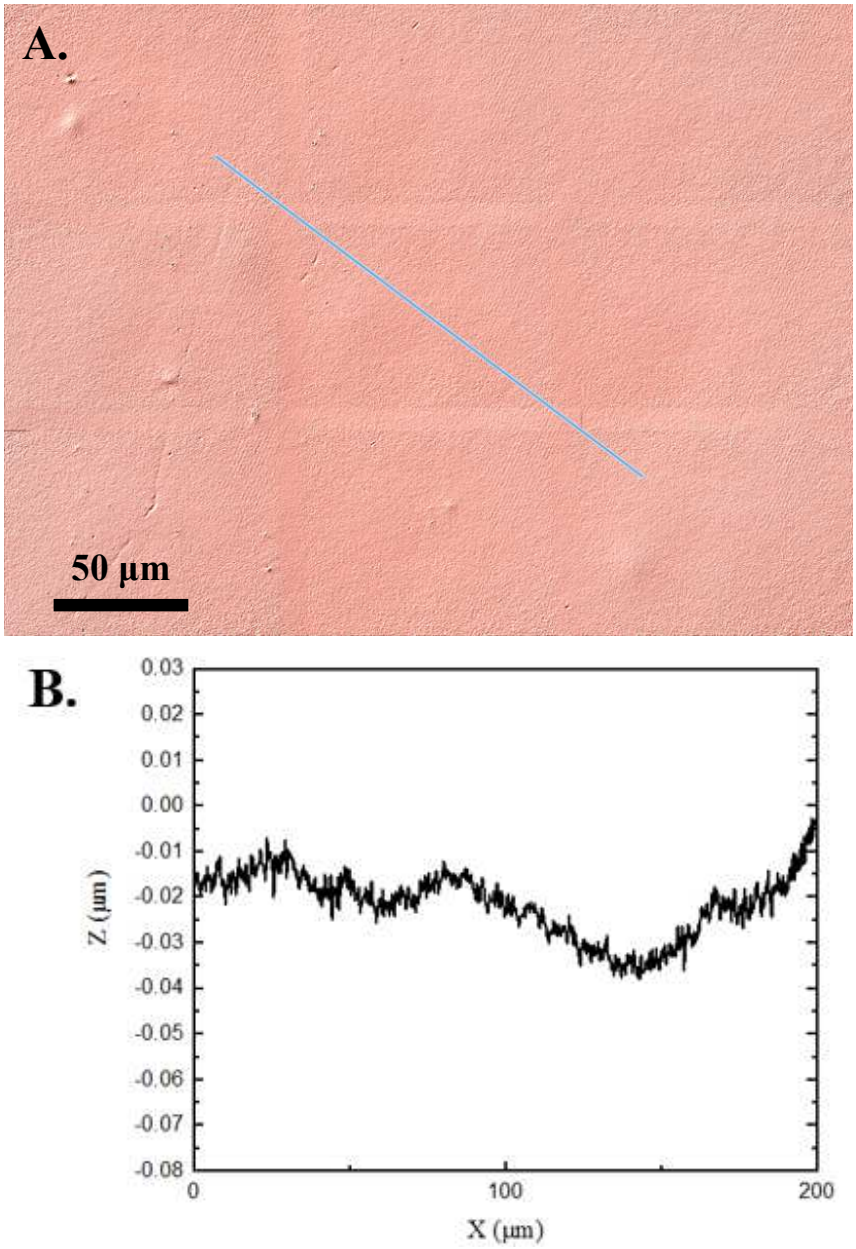

Figure 3.1: 3D confocal microscopy analysis of a control PDMS sample. (A) The surface is visibly flat with some minor surface impurities. (B) Graphical height displacement across an arbitrary line in the surface.

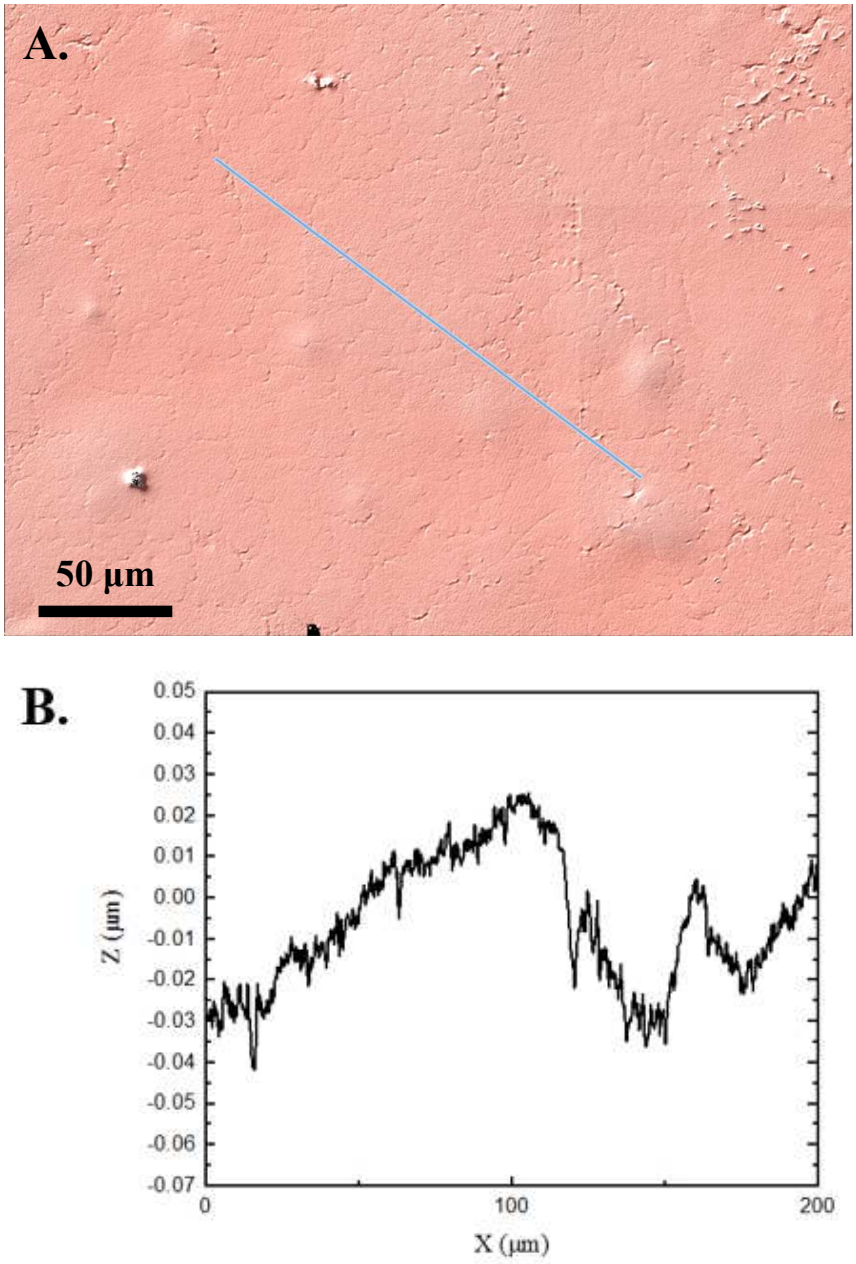

Figure 3.2: 3D confocal microscopy analysis of a typical experimental PDMS sample. (A) The surface shows patterns of wear that are distinct from the control visual. There appears to be some minor surface impurities. (B) Graphical height displacement across an arbitrary line in the surface.

The skewness (*Ssk*) is a dimensionless roughness parameter which also helps characterize the topography changes. A positive value of *Ssk* describes a height distribution that is below the mean plane, that is, the valleys create more of a bias than the peaks. A negative *Ssk* value

resembles a bias toward the peaks in the sample. Our hypothesis was that cavitation would create cavities in the surface, yielding a positive *Ssk* value. Hypothetically the control samples would ideally have an *Ssk* value at or around zero. The results align with our hypothesis with a control and experimental average *Ssk* value of 1.1 and 11.3, respectively. The positive *Ssk* value for the control sample is likely due to impurities that exist on the nanoscale during the curing process of PDMS[18]. The large *Ssk* value from the experimental samples points directly at an outside force creating erosion of the surface, similar to our anticipated hypothesis. This large *Ssk* also points to apparent cavitation damage because any debris or added noise that adheres to the surface by introducing the samples to the 1.5 gallon tank should cause a negative *Ssk* trend because they create peaks in the topography, but the cavitation erosion overrides this noise and remains biased below the mean height plane. Figure 3.3 highlights the collected *Sa* and *Ssk* values from the control and experimental samples using 3D confocal microscopy.

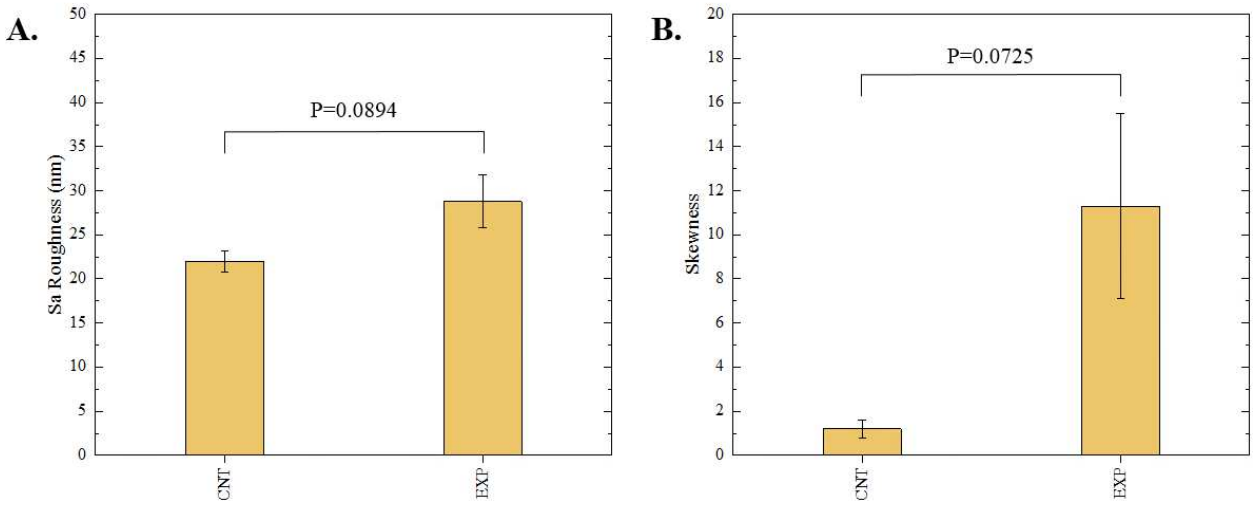

Figure 3.3: Summary of (A) average Sa, and (B) average Ssk roughness parameters of control and experimental samples via 3D confocal microscopy techniques. Error bars represent the standard error of the mean.

3.3.2 Interferometry

Interferometry methods offer another optical method for investigating and upholding the differences shown between the control and experimental samples in the 3D confocal microscopy methods. Figures 3.4&3.5 show illustrations of a typical control and experimental sample, respectively, via interferometry. Similar to 3D confocal microscopy, there is an apparent difference in the visual representation of the two surfaces. Noticeable wear and erosion is present on the control sample. Figures 3.4B&3.5B graphically represent the height of the surface along an arbitrary path. Both samples show noise and fluctuation in the surface height but only the experimental sample shows any sharp changes in the negative z-direction. This is significant because cavitation is theorized to cause nanoscale cavities with similar dimension in other biomedical applications [19]. Any dust or debris added to the surface through the controlled cavitation process should show an additive height, not a subtractive difference. Cavitation seems to be the only logical source of porous characteristics in the surface. Using interferometry techniques the average Sa values for control and experimental samples are 45.7 nm and 90.0 nm, respectively. Additionally, the average *Ssk* value for the control samples is 0.3, compared to an average *Ssk* value of 5.3 for experimental samples. Figure 3.6 summarizes the *Sa* and *Ssk* results from the control and experimental samples using interferometry. All in all these trends demonstrate a rougher surface for experimental samples that have bias below the mean height plane, similar to the results from 3D confocal microscopy techniques.

Some experimental samples from both 3D confocal microscopy and interferometry yield similar roughness parameters compared to the mean values of the control samples, while others show distinct change. This is likely due to the random positioning of MB adherence and induced cavitation which leads to varied damage across the PDMS films, hence a larger standard error of

the mean for experimental samples. Topographical analytics were collected randomly across the samples in order to eliminate visual bias. Overall trends point to clear topographical differences between the control and experimental samples using both 3D confocal microscopy and interferometry. This proven surface damage to a soft polymer with a slightly larger hardness of the human brain brings alarming awareness to the application of TBIs.

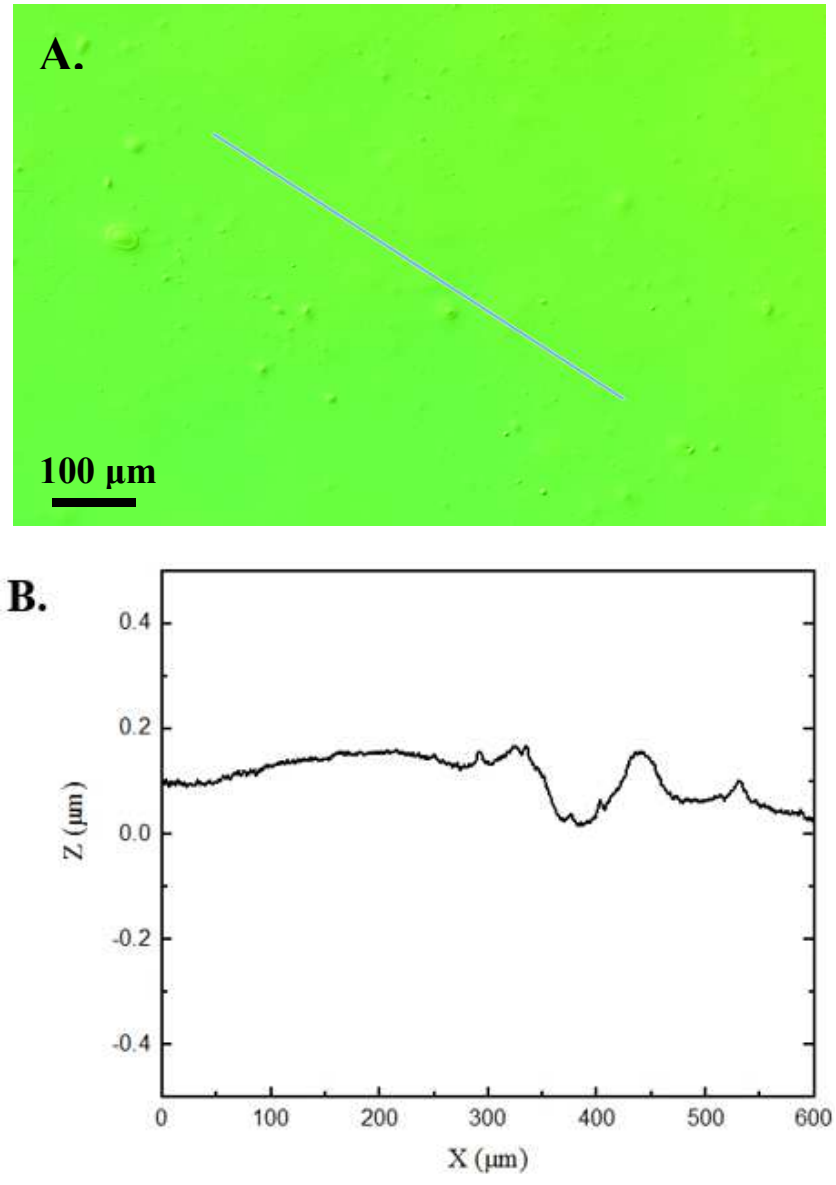

Figure 3.4: Interferometry analysis of a control PDMS sample. (A) The surface is visibly flat with some minor surface impurities. (B) Graphical height displacement across an arbitrary line in the surface. Any abrupt spikes in the z direction appear to be above the surface.

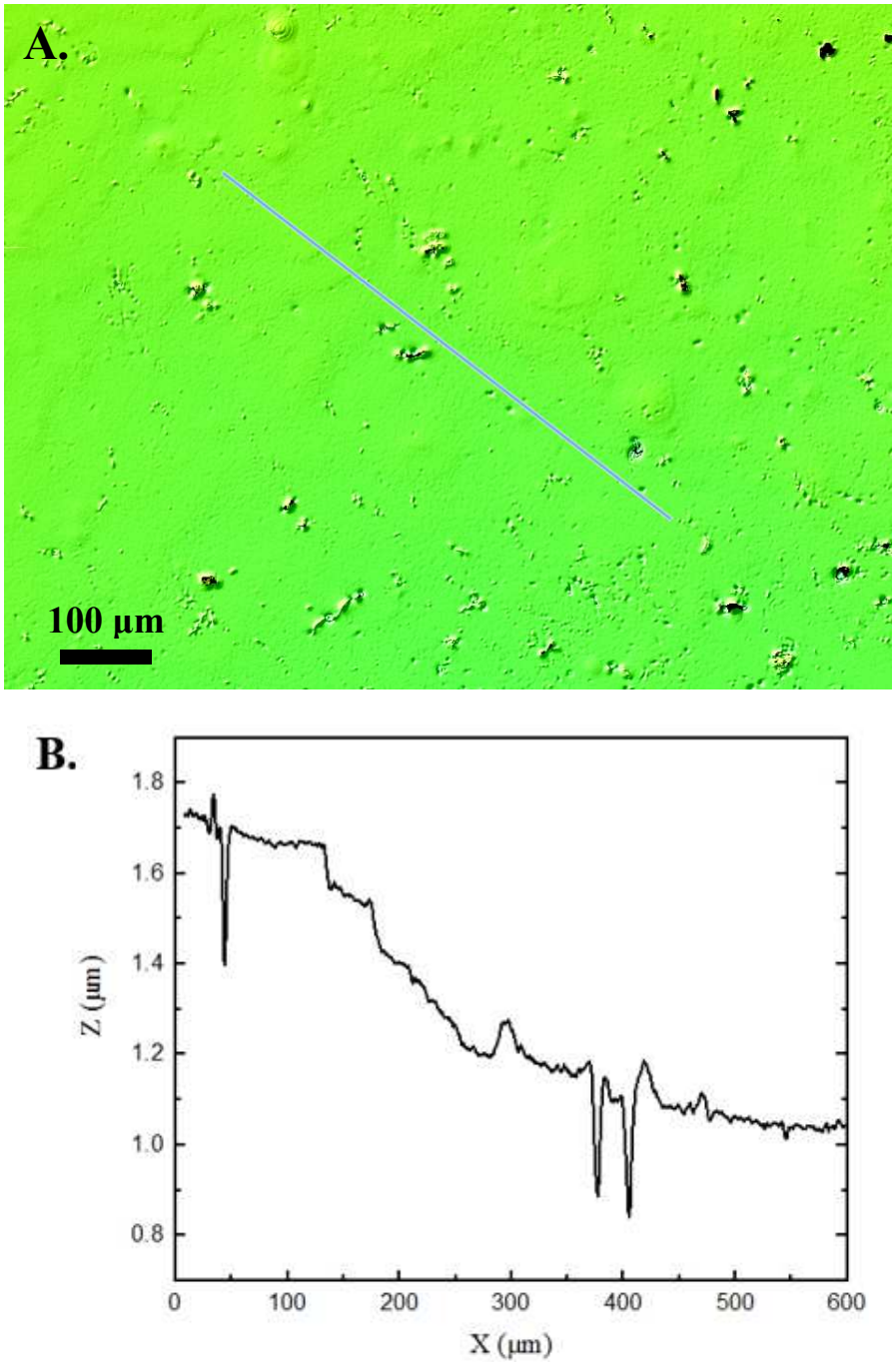

Figure 3.5: Interferometry analysis of an experimental PDMS sample. (A) The surface has a roughness texture that is visually different that the control images. (B) The graphical height displacement across an arbitrary line in the surface shows abrupt spikes in the z direction below the surface, points to signs of cavitation damage.

Characterizing the response of cranial anatomy to surrounding cavitation is the next step for future studies. Pharmacists can only provide the best treatment if cellular response to this TBI

phenomena is known. On top of this, if cellular damage shows catastrophic trends from cavitation exposure then engineers now realize the importance of eliminating or minimizing the possibility of cavitation existence in helmet design. All in all, this study has demonstrated the detriments that cavitation has on soft surfaces and helped motivate the progression of TBI knowledge.

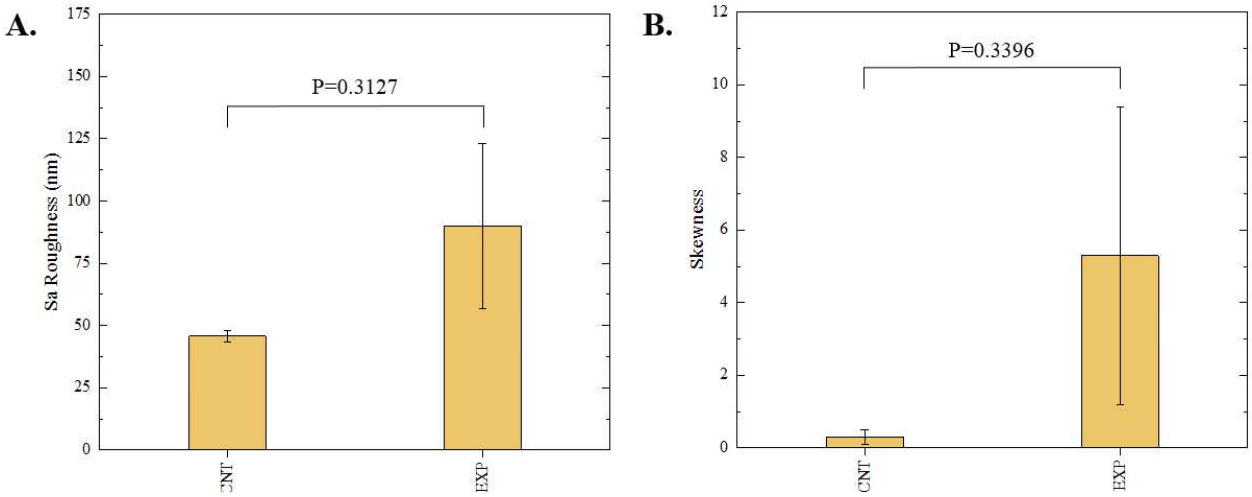

Figure 3.6: Summary of (A) average Sa, and (B) average Ssk roughness parameters of control and experimental samples via interferometry techniques. Error bars represent the standard error of the mean.

3.4 Conclusion

Cavitation is commonly known to exist and erode away nearby surfaces in a variety of applications, like propulsion and hydrodynamic pumping[9, 10, 13]. Recent theories have concluded that cavitation exists in the brain during a TBI and has the potential to leave behind detrimental effects[5, 6]. This study uses an existing apparatus that simulates controlled cavitation and analyzes the damages that soft polymers undergo after exposure to surrounding cavitation. Methods of 3D confocal microscopy and interferometry are used to study the surface topography of control and experimental samples. Comparative results conclude that induced

cavitation leads to clear damage and erosion to a PDMS surface. Although the PDMS samples do not exactly replicate the damage that the human brain might experience, it is clear that damage occurs in our simulations and this raises concern for how detrimental cavitation is on vulnerable cranial anatomy. Future studies seek to focus on the response that neuronal cells have to similar simulations of controlled cavitation. Taken together, this study has clear novelty that helps unmask the highly unknown characteristics of TBIs, allowing for advancements in providing better care and treatment to its victims.

References

[1] A. Chanda, C. Callaway, C. Clifton, and V. Unnikrishnan, "Biofidelic human brain tissue surrogates," vol. 25, ed: Mechanics of Advanced Materials and Structures, 2018, pp. 1335-1341.

[2] S. T. DeKosky, M. D. Ikonomovic, and S. Gandy, "Traumatic Brain Injury — Football, Warfare, and Long-Term Effects," vol. 363 ed: The New England Journal of Medicine, 2010, pp. 1293-1296.

[3] J. L. Zamanian *et al.*, "Genomic Analysis of Reactive Astrogliosis," vol. 32, ed: Journal of Neuroscience, 2012, pp. 6391-6410.

[4] S. Bartyczak and W. Mock, "Characterization of viscoelastic materials for low-magnitude blast mitigation," vol. 500, ed: Journal of Physics: Conference Series, 2014.

[5] J. Goeller, A. Wardlaw, D. Treichler, J. O'Bruda, and G. Weiss, "Investigation of cavitation as a possible damage mechanism in blast-induced traumatic brain injury," vol. 29, ed: Journal of Neurotrauma, 2012, pp. 1970-1981.

[6] M. B. Panzer, B. S. Myers, B. P. Capehart, and C. R. Bass, "Development of a finite element model for blast brain injury and the effects of CSF cavitation," vol. 40, ed: Annals of Biomedical Engineering, 2012, pp. 1530-1544.

[7] S. Haniff and P. A. Taylor, "In silico investigation of blast-induced intracranial fluid cavitation as it potentially leads to traumatic brain injury," vol. 27, ed: Shock Waves, 2017, pp. 929-945.

[8] P. A. Taylor, J. S. Ludwigsen, and C. C. Ford, "Investigation of blast-induced traumatic brain injury," vol. 28, ed: Brain Injury, 2014, pp. 879-895.

[9] J. Bin, L. Xianwu, and Y. Wu, "Unsteady cavitation characteristics and alleviation of pressure fluctuations around marine propellers with different skew angles," vol. 28, ed: Journal of Mechanical Science and Technology, 2014, pp. 1339-1348.

[10] B. K. Sreedhar, S. K. Albert, and A. B. Pandit, "Cavitation damage: Theory and measurements – A review," vol. 372-373, ed: Wear, 2017, pp. 177-196.

[11] M. Petkovsek and M. Dular, "Simultaneous observation of cavitation structures and cavitation erosion," vol. 300, ed: Wear, 2013, pp. 55-64.

[12] E. Herbert, S. Baliber, and F. Caupin, "Cavitation pressure in water," vol. 74, ed: Physical Review. E. Statistical, Nonlinear, and Soft Matter Physics, 2006, p. 041603.

[13] L. Chernin and D. V. Val, "Probabilistic prediction of cavitation on rotor blades of tidal stream turbines," vol. 113, ed: Renewable Energy, 2017, pp. 688-696.

[14] K. Y. Lee and D. J. Mooney, "Hydrogels for Tissue Engineering," vol. 101, ed: Chemical Reviews, 2001, pp. 1869-1879.

[15] M. Cabello *et al.*, "Electrostimulation in an autonomous culture lab-on-chip provides neuroprotection of a retinal explant from a retinitis pigmentosa mouse-model," vol. 288, ed: Sensors and Actuators B-Chemical, 2019, pp. 337-346.

[16] A. H. Wrede, A. Shah, M. C. McNamara, R. Montazami, and N. N. Hashemi, "Controlled positioning of microbubbles and induced cavitation using a dualfrequency transducer and microfiber adhesion techniques," vol. 43, ed: Ultrasonics Sonochemistry, 2018, pp. 114-119.

[17] E. S. Gadelmawla, M. M. Koura, T. M. A. Maksoud, I. M. Elewa, and H. H. Soliman, "Roughness Parameters," vol. 123, ed. Journal of Materials Processing Technology, 2002, pp. 133-145.

[18] C. Con and B. Cui, "Effect of mold treatment by solvent on PDMS molding into nanoholes," vol. 8, ed: Nanoscale Research Letters, 2013.

[19] Y. Zhou, K. Yang, J. Cui, J. Y. Ye, and C. X. Deng, "Controlled permeation of cell membrane by single bubble acoustic cavitation," *Journal of Controlled Release,* vol. 157, no. 1, pp. 103-111, 2012.

CHAPTER 4. CHARACTERIZATION OF ASTROCYTIC RESPONSE AFTER EXPERIENCING ACOUSTICALLY-INDUCED CAVITATION IN VITRO

Modified from a manuscript submitted in Global Challenges

Alex H. Wrede[1], Marilyn C. McNamara[1], Rodger Baldwin[1], Jie Luo[2], Reza Montazami[1], Anumantha Kanthasamy[2], and Nicole N. Hashemi[1,2]*

[1] Department of Mechanical Engineering, Iowa State University, Ames, Iowa 50011, USA

[2] Department of Biomedical Sciences, Iowa State University, Ames, IA 50011, USA

Abstract

When a traumatic brain injury (TBI) occurs, low-pressure regions inside the skull can cause vapor contents in the cerebral spinal fluid (CSF) to expand and collapse, a phenomenon known as cavitation. During cavitation, emitted shock waves are theorized to have alarming adverse effects on surrounding anatomy. We create cavitation via acoustics by making advancements on a previously engineered system. Using cell-laden microfibers we visually analyze the longitudinal morphological response that mouse astrocytes portray after cavitation exposure. Morphological damage was evident immediately after cavitation when compared to a control sample, as cellular processes retracted. Forty-eight hours later the astrocytes appeared cultured across the fibers, as normal. Gene expression changes that occur post-cavitation are also analyzed via quantitative polymerase chain reaction (qPCR) methods. After cavitation a number of pro-inflammatory genes were upregulated, including, TNFα, IL-1β, C1q, Serping1, NOS1, IL-

6, and JMJD3. Taken together these results characterize the detrimental effects that surrounding cavitation has on astrocytic function, and yield advancements for TBI care and prevention practices.

4.1 Introduction

Traumatic brain injuries (TBIs) are a large problem in modern society. Estimates show that by the year 2020, TBIs will become the third most prevalent cause of death worldwide.[1] TBIs have two different stages of injury: primary and secondary. A primary injury occurs at the time of the injury, which might be a skull fracture, force-related stress from the brain shifting within the skull boundary, or cavitation, which is the formation and dramatic collapse of MBs. A secondary injury occurs sometime after the injury, such as intracranial inflammation or blood-brain barrier damage.[2, 3] This study aims to specifically focus on the damages that the primary injury of cavitation has on surrounding neuronal cells and seeks to elucidate the unknown nature and unpredictability of TBIs.

The existence of cavitation inside the skull during a TBI situation is a modern hypothesis in research. Goeller et al. used a brain-like ellipsoid model in a shock tube to confirm the existence of cavitation in a TBI environment.[4] During a blast-TBI, the initial compressive wave travels through the skull and a fraction of this wave reflects off impedance boundaries, resulting in a negative pressure reflection wave.[5] It is in these low pressure regions where intracranial cavitation exists.[6, 7] The CSF has minute pockets of vapor because of its primary components, which are oxygen, nitrogen, and water vapor.[8] When these vapor pockets are exposed to low pressure conditions they dramatically expand and collapse when the bubble radius exits the stability region.[9] This expansion and collapse creates an intense localized force

measured anywhere from 0.1-20 MPa.[10] Cavitation damage has been heavily investigated in mechanical pump and watercraft propulsion applications.[11-13] Characterization of the impact that cavitation has inside the skull during a TBI remains to be fully explored and thus is the ultimate novelty of this study. [14]

On top of TBIs, there are other profound neurological disorders, such as, Alzheimer's disease, Parkinson's disease, and psychiatric diseases, affecting large portions of the population. Research has shown a pro-inflammatory response in the pathogenesis during these situations.[15, 16] Astrocyte activation plays a vital role in initiating neuroinflammation.[17, 18] Astrocytes are bountiful in the CNS and provide a variety of functions in the neuronal network, such as, supplying support and structure to neurons, and enhancing synapse formation and function.[19] Upon insult, though, the full functionality of astrocytes may be lost. Previous research has categorized astrocyte reactivity into two groupings, called A1 and A2 astrocytes.[18] A1 astrocytes are the result of an inflammatory response similar to what is observed during a blast-TBI, and are known to be harmful because they lose regular astrocytic functionality and instead provide a neurotoxic function that kills neurons. A1 astrocytes upregulate many genes that are known to be damaging to synapses. However, A2 astrocytes, which are activated through ischemia, are shown to be protective by further promoting CNS repair and recovery.[20-22] We postulate that cavitation will induce astrocytes to represent the A1 astrocyte phenotype and upregulate mostly A1 specific genes. Because of the large role that astrocyte cells play in TBI response, this study is solely focused on the investigation of astrocyte activation in response to surrounding cavitation. Future studies involving co-cultures of multiple types of neuronal cells will further elucidate this phenomenon by lending further physiological relevancy.

Neuronal cells are also known to retract their processes during a blast-TBI.[23] The

model analyzed in our study demonstrates this retraction function in astrocytes by conducting a time-dependent visual study of cells at different stages post cavitation. We compare this collage with a control sample to demonstrate that cavitation is a primary inducer for astrocytes to portray an amoeboid morphology. These results motivated a genetic study to further investigate the A1 vs A2 expressions in astrocytes post-cavitation. Our hypothesis is that the astrocytes that experience damage from surrounding cavitation will represent the phenotype of A1 astrocytes because this is an inflammatory insult. Some classic genes that show upregulation in pro-inflammatory astrocytes include, Tumor Necrosis Factor alpha (TNFα), Interleukin 1-beta (IL-1β), C1q, Serping1, and other reactive oxygen species.[24-27] Related studies conclude that unknown oxygen species are secreted by astrocytes and in turn, act as neurotoxins.[28] Nitric oxide (NO), more specifically neuronal nitric oxide synthase (NOS1), plays a vital role in the overall function of the CNS.[29] In neurodegenerative diseases like Parkinson's disease[30], stroke[31], Alzheimer's disease[32], and amyotrophic lateral sclerosis[33], there has been evidence of increased NOS1 expression.[29] It has been proven that increasing concentrations of TNFα and IL-1β also increases the presence of interleukin 6 (IL-6) in mouse astrocytes.[23] This trend is magnified in human astrocytes.[34] IL-6 has also been associated with multiple sclerosis (MS).[35] An increased concentration of jumonji domain containing 3 (JMJD3) also has been proven to lead to upregulation in IL-6.[36] On top of this, increasing levels of JMJD3 has been shown to activate the expression of a variety of pro-inflammatory genes in neuronal cultures.[17, 36] This study focuses on characterizing the expression of TNFα, IL-1β, C1q, Serping1, NOS1, IL-6, and JMJD3 in mouse astrocytes cells after experiencing surrounding cavitation. We also wanted to analyze some anti-inflammatory (A2 phenotype) genes to see if cavitation solely had influence on A1 specific genes. The well-known anti-inflammatory genes

that we test are tm4sf1, sphk1, CD14, IL13, and Arginase1.[18, 25, 27, 37] For all of our gene expression studies we used qPCR methods. A detailed summary of these gene expression changes has the potential to unmask important specifics about the nature of TBI at the cellular level.

Previous studies have designed an apparatus that creates controlled cavitation. This process produces, traps, positions, and collapses MBs arbitrarily in a tank using microfiber adhesion and an ultrasound transducer. This apparatus was also designed to realistically mimic the cavitation phenomena that exists during a TBI.[38] Our study seeks to advance this design by making it bio-compatible and sterile for cell incorporation. Introducing astrocytes in this apparatus and performing visual and gene expression analytic techniques, we demonstrate that cavitation has an adverse effect on astrocytic morphology and genetics.

4.2 Materials and Methods

4.2.1 Biocompatibility and Sterilization

Previous studies describe the apparatus we use to create controlled cavitation by having the ability to arbitrarily produce, trap, position, and collapse MBs.[38] In order to make this apparatus sterile and stable for live cellular testing there are multiple advancements that were implemented. Traditionally cellular testing is done underneath a sterilized fume hood but with the necessary components for MB creation, positioning, and collapse, conducting experiments under a fume hood for this project is impractical. The 3-axis stages and high-speed camera are mounted onto an optics table in order to remain stationary, which a biological fume hood environment is unable to provide. In order to obtain sterility and stability for cellular analysis we

made a number of advancements. The 1.5 gallon tank was filled with 3.5 liters of phosphate buffered saline (PBS) instead of deionized water to account for cell compatibility. Before the PBS was put into the tank, the tank was first sprayed down with 70% ethanol and put in a sterilized fume hood until dry under UV. Then the PBS was poured into the tank under the fume hood and exposed to 45 minutes of UV light for further sterilization. Also, the pieces of the mechanical arm that was submerged in the PBS and used to hold the polycaprolactone (PCL) frame stationary between the capillary tubing and transducer were also sterilized with 70% ethanol and exposed to UV light for 45 minutes. The surrounding shelves and walls were also draped with sterilized plastic to eliminate any dust or debris falling into the tank during experimentation. Additionally, all other surrounding components (capillary tubing, 3-axis stage, transducer and the mechanical arm that held it stationary, and the transducer cords) were sprayed and wiped with 70% ethanol continuously prior to the introduction of cells. After the PBS filled tank was sterilized, it was then covered with a sterile sheet and placed in an oven to heat at 70 °C for 1 hour. This allowed for the PBS to warm to about body temperature so the cells would not experience a temperature shock when being introduced in the tank. The cell-laden fiber frames were kept in a sterile and stable incubator before and after trials. Using these advancements, we were able to eliminate any signs of infection or contamination in all of our samples.

4.2.2 Fibrous Frame Fabrication

We fabricated frames by encapsulating copper within Polydimethylsiloxane (PDMS) (1:10 Base:Elastomer) in a ‘U’ shape, since exposed copper caused cell death and PDMS floated within the media and exposed fibers to the air. Fibers were fabricated using a well-documented protocol involving a microfluidic device.[39, 40] Specifically, 5% PCL (M_n = 80,000, Sigma-

Aldrich, St. Louis, MO) was dissolved into 2,2,2-Trifluoroethanol (TFE, Oakwood Chemical, West Columbia, SC) to form the core solution, while 5% Poly-ethylene glycol (M_n = 20,000, Sigma-Aldrich, St. Louis, MO) was dissolved into a 1:1 solution of DI water and ethanol for a sheath fluid. Fibers were the result of a 5:75 μL/min: μL/min flow rate ratio. Fibers were wrapped around the aforementioned frames in a ratio of 10 fibers per frame.

4.2.3 Cell Model

The mouse astrocytes (CRL-2541) used in this project were purchased from American Type Culture Collection (ATCC, Manassas, VA) because of their known utility in TBI studies.[41] The cells were grown according to company protocol in growth media (ATCC, 30-2002). The culture media was also supplemented with 10% FBS and 1% penicillin (10,000 U/mL)- streptomycin (10,000 μg/mL), both of which were purchased from Gibco (Waltham, MA). The cells in all of our data collection consist of culture passage numbers 3-7. The astrocytes were housed in an incubator set at 37 °C with 5% CO_2.

4.2.4 Visual Morphology Analysis

We seeded cells onto biocompatible PCL microfibers (Hashemi Lab, Iowa State University, Ames, IA) to promote cell adhesion and allow for groupings of finite amounts of cells.[42, 43] The cells were suspended at a density of $1.06 * 10^6$ cells/mL before 0.25 mL of cells were introduced to the fibers and cultured overnight prior to running experiments. A large fraction of the seeded cells settled on the bottom of the culture flask but some adhered to the microfibers. The apparatus layout for our technique was similar to that of the microfiber adhesion technique documented in previous studies.[38] The function generator input settings for

the ultrasonic cavitation induction were: center frequency 100 kHz, 5 cycles, pulse repetition frequency 59 Hz, 130 Vpp. The culture tank is filled with PBS and has a measured pH value of 7.35. Using the microfiber adhesion method we have arbitrary control over the number of MBs that are captured on the cell-laden microfibers. All images of MBs adhered to cell-laden microfibers are captured using a long-distance microscope (Model K2, Infinity Photo-Optical Company) in unison with a high speed camera for imaging (BlackFly, FLIR) while the samples are in the 1.5 gallon tank. After cavitation, the samples were placed in 12-well plates and all images are captured using an inverted microscope (Zeiss, Germany). A growth analysis was conducted in order to quantify the changes that are observed between the experimental and control samples. The total area of growth in the plane of the inverted microscope was quantified and measured using imageJ software (Wayne Rasband, NIH).

4.2.5 Gene Expression Analysis via qPCR

The apparatus configuration of this experiment is similar to that of the visual morphology analysis, but with one slight modification, the cells are seeded onto sterilized 12 mm coverslips instead of using microfiber scaffolds, shown in Figure 4.1.

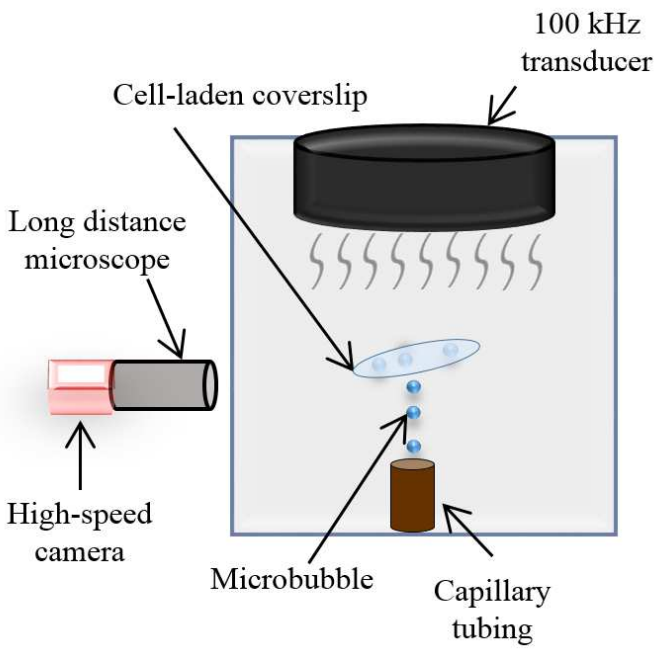

Figure 4.1: Apparatus configuration for genetic analysis. Coverslips are suspended using a mechanical arm that is stationed on a 3-axis stage, allowing for capture of MBs at arbitrary positions on the coverslip. When the coverslip has an optimal amount of adhered MBs on its underside, it is rotated 180° so the MBs and cells are exposed to the ultrasound.

The mouse astrocytes were seeded onto the coverslips at $1.17 * 10^6$ cells per coverslip and cultured overnight in the incubator prior to experimentation. There were 40 total seeded coverslips, 20 designated for a control sample and 20 designated for experimental sample. The cell-laden coverslips were suspended mid-solution with a tweezers clamped in a mechanical arm. Control samples were submerged in the PBS tank and exposed to ultrasound (center frequency 100 kHz, 5 cycles, pulse repetition frequency 59 Hz, 130 Vpp), but there were not any MBs present to produce cavitation. The experimental samples experienced an identical environment with the addition of 30-40 MBs adhered on each coverslip prior to activating the ultrasound. After the MBs are collected along the cell-seeded surface, the coverslips are then manually rotated 180° so the cells and MBs are aligned with beam of the transducer and cavitation is able to occur. After treatments the cell-laden coverslips were trypsinized, collected, combined to

create one control and one treatment sample, pelleted, and frozen at -80 °C until homogenization. Samples were homogenized in TRIzol reagent (Invitrogen Cat number: 15596026). RNA isolation was done following the TRIzol reagent manufacturer's protocol. Next, a cDNA synthesis system, High Capacity cDNA Reverse Transcription Kit, was used to complete a reverse transcription and convert the RNA to cDNA (Applied Biosystems, Foster City, CA). The relative magnitude of gene expression was measured using real-time PCR with Qiagen RT^2 SYBR Green master mix and validated Quantitect qPCR mouse primers from Qiagen (Frederick, MD). Mouse gene 18S rRNA (Qiagen Cat. No. PPM57735E) was used as the housekeeping gene, and used in the normalization of each sample. In order to ensure that florescence data from amplicon peaks were not from of any nonspecific amplicons, dissociation and melting curves were ran, according to the protocol from the manufacturer. The final results were calculated using the $\Delta\Delta C_t$ method and implementing the threshold cycle (C_t) value for the housekeeping gene and for the respective gene of interest in each sample. The reported expression changes are represented as fold changes between the control sample and treatment sample of each targeted gene.[44]

4.3 Results and Discussion

4.3.1 Visual Morphology Analysis

With our advanced apparatus, it is possible to achieve a wide range of control over the configuration of the microfiber-cell-MB complex. Figure 4.2 illustrates typical arrangements of trapped MBs next to clusters of cells in the apparatus. We have arbitrary control where the MBs adhere, the number of MBs that adhere, and the size of the MBs, because the microfiber scaffold is attached to a 3-axis stage and easily adjusted to enter the plane of the rising MBs, allowing for MBs to coalesce allows for varying MB sizes. In Figure 4.2C, a 60 μm bubble is adhered to the

cells on the top of the cell group and a larger MB around 100 microns is placed on the bottom of the grouping. The 100 µm bubble was created by allowing two 60 µm bubbles to coalesce.

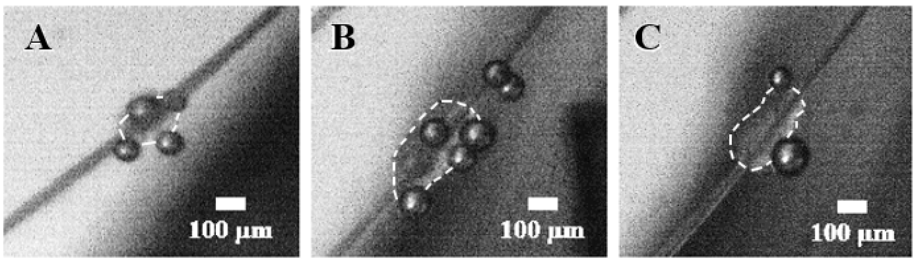

Figure 4.2 (A-C): Illustration of some different arrangements of MBs adhered to healthy clusters of astrocyte cells during experimentation. Dotted lines are shown to help outline clusters of cells. Higher magnification of cell morphology via an inverted microscope is shown in Figure 4.4. These images are taken with the samples inside the PBS tank.

After an arbitrary amount of MBs are collected on the cell-laden microfibers, the ultrasonic transducer is activated, resulting in cavitation. Figure 4.3 shows a collage that illustrates live cavitation on cell-laden microfibers.

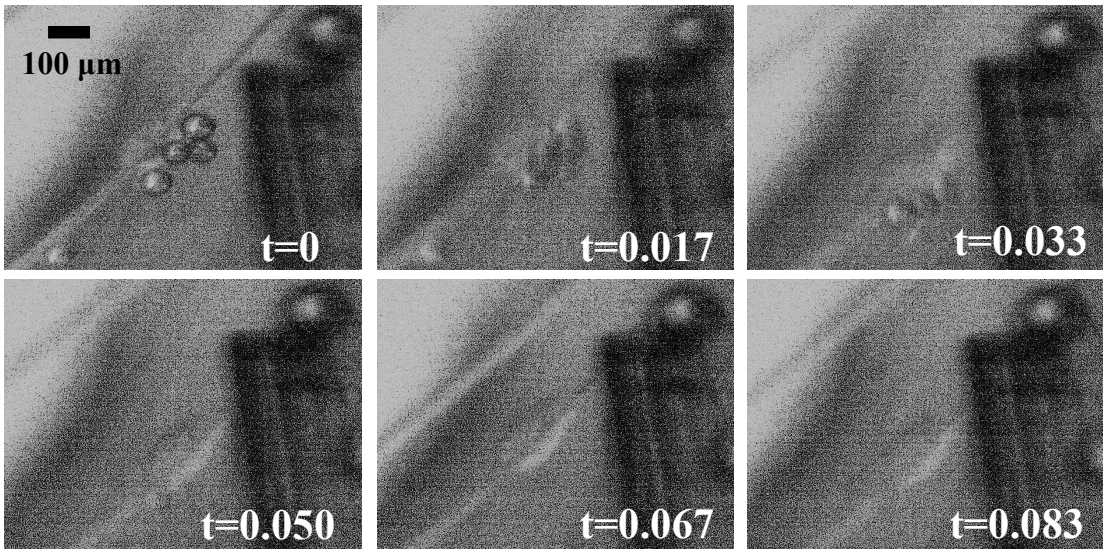

Figure 4.3: Longitudinal collage showing cavitation on cell-laden microfibers. The samples are in the PBS tank and pictures are taken with high-speed camera and telescopic lens. At t=0 the ultrasonic transducer is activated. The later frames show the dramatic oscillation and collapse of MBs in response to ultrasound exposure.

The astrocytic response is illustrated through a comparative analysis with a control and experimental sample in order to justify that cavitation is the leading contributor to inducing reactive astrocytes. The control sample was submerged in the PBS tank and also experiences ultrasound exposure from the transducer. There are not any adhered MBs on the control sample so cavitation does not exist when the transducer is activated. The experimental sample is exposed to PBS, ultrasound exposure, and surrounding cavitation because of the presence of adhered MBs prior to activating the ultrasonic transducer. Figures 4.4&4.5 show the longitudinal astrocytic response for the experimental and control samples, respectively. In Figure 4.4, this particular sample had five ~60 µm MBs adhered to the group of cells prior to activating the ultrasonic transducer.

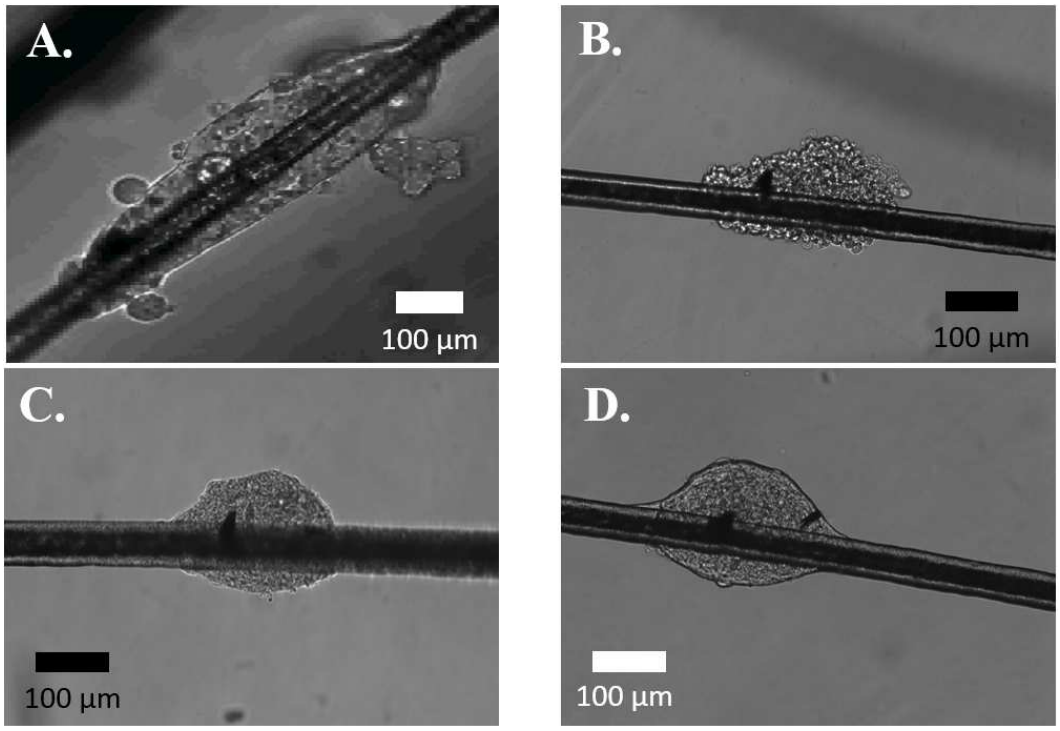

Figure 4.4: Visual analysis of mouse astrocyte response the cavitation. These images are captured via an inverted microscope outside of the PBS tank and the sample is in a cell culture plate. (A) Astrocyte sample before experiencing PBS, ultrasound, and cavitation exposure. After they are exposed, we visualize their response immediately after treatment (B), 22 hours after treatment (C), and 48 hours after treatment (D).

A growth analysis was done to quantify the retraction of processes and total surface area in both experimental and control samples. The results concluded that both samples increased in surface area 48 hours after control and experimental exposures, but the magnitude of growth was significantly different. The control sample (Figure 4.5) grew at a rate of 200% and the experimental sample (Figure 4.4) grew 109%, both over 48 hours. Figure 4.6 illustrates the astrocytic surface area growth in all of our trials.

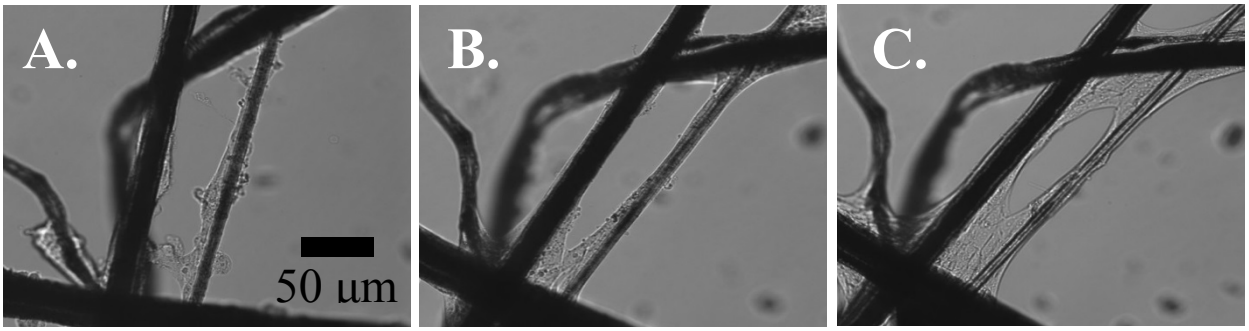

Figure 4.5: Visual analysis of astrocytic response to PBS and ultrasound exposure, but no exposure to cavitation. This sample is used as a control. (A) Represents the sample immediately after exposure, (B) represents the sample 22 hours after exposure, and (C) represents the sample 48 after exposure.

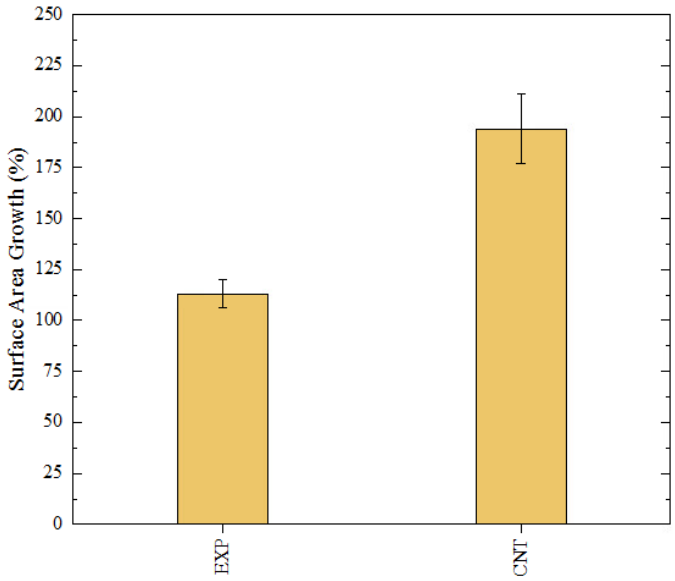

Figure 4.6: Growth analysis 48 hours after control and experimental exposures. Magnitudes are percentages relative to the area measured immediately after experiencing control or experimental conditions. Error bars represent ± 1 Standard Deviation.

4.3.2 Genetic Analysis via qPCR

Through our visual analysis studies we were able to see that astrocytes retract their processes immediately after exposure to cavitation and they begin to elongate overtime. We further investigate this response by studying the A1 and A2 genetic phenotype immediately after cavitation. This is done via qPCR methods and using the cDNA from the separated control and experimental samples. Figure 4.7 outlines the astrocyte phenotype represented by astrocytes that have been activated via cavitation. The A1 specific genes that we test are: TNFα, IL-1β, C1q, Serping1, NOS1, IL-6, and JMJD3. The A2 specific genes that we test are: tm4sf1, sphk1, CD14, IL13, and Arginase1. Expression values are represented as normalized fold changes from the control and treatment samples from each of these genes.

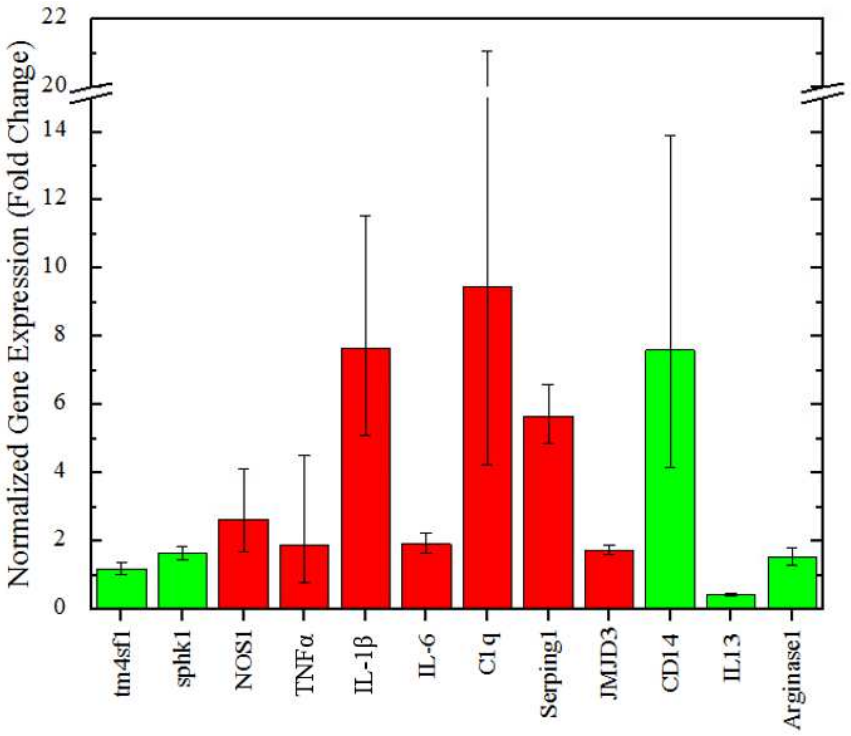

Figure 4.7: Gene expression analysis of mouse astrocytes immediately after exposure to surrounding cavitation in the PBS tank. Expressions are represented as a fold change between the control sample and treatment sample of each targeted gene. Genes labeled with red bars designate A1 specific genes and genes labeled with green bars designate A2 specific genes.

The presence of cavitation inside the skull during a TBI is a modern hypothesis. Some studies have recently proven the existence of this phenomenon[4, 45], but there is limited knowledge on the characterization of cellular response in this scenario. This study used controlled cavitation techniques from previous studies and made modifications and advancements in order to obtain biocompatibility and sterility, allowing for the incorporation of mouse astrocytes.[38] We used astrocytes in this study because of their documented role in TBI response and recovery.[18, 28] Future studies aim to incorporate multiple types of neuronal cells in order to further characterize the damages that cranial cavitation has on surrounding anatomy.

One of the novelties of this study is ability to visualize the cellular response of a finite amount of cells by using cell-laden microfibers. In the visual analysis we were able to see morphology differences between control and experimental samples. In the experimental sample the astrocytes clearly retract their processes and represent an amoeboid morphology. This is shown in Figure 4.4B where the cell grouping has a very rough surface. In the control sample there is also some evident cellular disruption (Figure 4.5A) but the cells appear displaced, instead of damaged. The outer boundaries of the cell groupings do not have this rough nature, like the experimental sample. The displacement of cells in the control sample is likely due to the transportation of the sample from the PBS tank to cell culture plate. After 22 and 48 hours both samples appear to expand their processes and spread across the fibers. For both experimental and control samples the total measured surface area increases 48 hours after relative exposures, however, the control samples grow significantly faster compared to the experimental samples. This dramatic increase in surface area for the control samples is likely due to the astrocytic function of forming protective scar tissue when entering the PBS tank.[46] A1 astrocytes lose this functionality and no longer protect surrounding neurons.[18]

Given the difference in morphology immediately after experimental and control exposures, we sought to investigate the genetic differences at this time point. Future studies aim to characterize the genetic tendencies longitudinally, for it is known that genetic phenotypes change overtime.[46] Current technology is limited in offering analytic techniques to gather genetic phenotypes of small amounts of cells, like the cell groupings on microfibers. Techniques like qPCR require large amounts of cells due to sensitivity constraints. Single-cell RNA sequencing is an evolving method that offers this ability but we have limited access and resources to pursue this technique. We instead engineered our apparatus to allow for greater amounts of cells and the incorporation of qPCR. We did this by replacing the cell-laden microfiber scaffold with sterilized cell-seeded coverslips. Due to the increase in cell amount and sample area, we also increased the number of adhered MBs to 30-40 per sample instead of 5-10, like what was adhered to the cell-laden microfibers. The gene expression results show a clear difference between experimental and control phenotypes. All selected A1 markers were unregulated after cavitation. The following genes also had at least +2 fold change: IL-1β, C1q, Serping1, and NOS1, analogous to literature.[18, 28, 29] Of the A2 markers that were tested, the only A2 gene that was unregulated with a fold change of 2+ was CD14. These A1 and A2 genetic findings lead us to conclude that surrounding cavitation induces A1 reactive astrocytes and in turn, can be detrimental to the neuronal network. It is aforementioned that NOS1 expression is directly correlated to the presence of neurodegenerative diseases.[29-33] Increased levels TNFα, IL-1β, and JMJD3 spike the levels of IL-6 and, in turn, has been directly associated with MS.[23, 35, 36] Our genetic findings are significant because if cavitation is proven to be a leading contributor in A1 induction then this provides another avenue in preventative care. The pharmaceutical attention goes toward curing the damage that A1

astrocytes endow, but the engineering attention can now have a focus in studying where cavitation specifically occurs in the brain. A location map of cavitation occurrence can be directly used to design a helmet that dampens force and reduces the possibility of cavitation, which in turn, reduces neurotoxicity in astrocytic response and minimizes TBI detriments.

4.4 Conclusion

TBIs are complex injuries that often times lead to unpredictable symptoms for its victims. There are primary and secondary injuries that occur during a TBI. Breaking down these injuries and studying the effects that they endow on the cellular levels is important in order to gain knowledge on the topic. An example of a primary injury is cavitation that exists in low pressure regions of the brain. We made advancements to an apparatus designed in previous studies that creates, traps, positions, and collapses MBs that realistically resemble those in a blast-TBI event.[38] Our study uses PCL microfibers to mimic a biocompatible and sterile neuronal environment for mouse astrocyte cells in-vitro. We document a visual study that demonstrates surrounding cavitation has a profound effect on astrocytic activation. We also use qPCR techniques to investigate the effects that surrounding cavitation has on the genetic phenotype of astrocytes. This study has proven that astrocytic function drastically changes upon exposure to surrounding cavitation. A1 genetic tendencies are consistently represented and known to be neurotoxic. This study can be used as a platform in efforts to eliminate cavitation in the brain through advanced helmet design. Further research focusing on the response of multiple types of neuronal cells after experiencing surrounding cavitation will be vital in continuing the advancement to TBI prevention and care.

References

[1] D. F. Meaney, B. Morrison, and C. D. Bass, "The Mechanics of Traumatic Brain Injury: A Review of What We Know and What We Need to Know for Reducing Its Societal Burden," vol. 136, ed: Journal of Biomechanical Engineering, 2014, 021008.

[2] H. L. Tian *et al.*, "Risk factors for posttraumatic cerebral infarction in patients with moderate or severe head trauma," vol. 31, ed: Neurosurgical Review, 2008, pp. 431-437.

[3] N. B. Topal *et al.*, "MR imaging in the detection of diffuse axonal injury with mild traumatic brain injury," vol. 30, ed: Neurological Research, 2008, pp. 974-978.

[4] J. Goeller, A. Wardlaw, D. Treichler, J. O'Bruda, and G. Weiss, "Investigation of cavitation as a possible damage mechanism in blast-induced traumatic brain injury," vol. 29, ed: Journal of Neurotrauma, 2012, pp. 1970-1981.

[5] J. D. Achenbach, *Wave Propagation in Elastic Solids*. NY, USA: North Holland Publishing Company; American Elsevier Publishing Company, 1973.

[6] R. S. Salzar, D. Treichler, A. Wardlaw, G. Weiss, and J. Goeller, "Experimental Investigation of Cavitation as a Possible Damage Mechanism in Blast-Induced Traumatic Brain Injury in Post-Mortem Human Subject Heads," vol. 34, ed: Journal of Neurotrauma, 2017, pp. 1589-1602.

[7] S. Canchi, K. Kelly, Y. Hong, M. A. King, G. Subhash, and M. Sarntinoranont, "Controlled single bubble cavitation collapse results in jet-induced injury in brain tissue," vol. 74, ed: Journal of the Mechanical Behavior of Biomedical Materials, 2017, pp. 261-273.

[8] S. Haniff and P. A. Taylor, "In silico investigation of blast-induced intracranial fluid cavitation as it potentially leads to traumatic brain injury," vol. 27, ed: Shock Waves, 2017, pp. 929-945.

[9] A. Shima, "Studies on bubble dynamics," vol. 7, ed: Shock Waves, 1997, pp. 33-42.

[10] E. Herbert, S. Baliber, and F. Caupin, "Cavitation pressure in water," vol. 74, ed: Physical Review. E. Statistical, Nonlinear, and Soft Matter Physics, 2006, 041603.

[11] A. Philipp and W. Lauterborn, "Cavitation erosion by single laser-produced bubbles," vol. 361, ed: Journal of Fluid Mechanics, 1998, pp. 75-116.

[12] L. Chernin and D. V. Val, "Probabilistic prediction of cavitation on rotor blades of tidal stream turbines," vol. 113, ed: Renewable Energy, 2017, pp. 688-696.

[13] J. Bin, L. Xianwu, and Y. Wu, "Unsteady cavitation characteristics and alleviation of pressure fluctuations around marine propellers with different skew angles," vol. 28, ed: Journal of Mechanical Science and Technology, 2014, pp. 1339-1348.

[14] C. Franck, "Microcavitation: the key to modeling blast traumatic brain injury?," vol. 2, ed: Concussion, 2017, p. 3.

[15] R. M. Ransohoff and J. E. Khoury, "Microglia in Health and Disease," vol. 8, ed: Cold Spring Harbor Perspectives in Biology, 2015, p. 1.

[16] A. Bhattacharya, N. C. Derecki, T. W. Lovenberg, and W. C. Drevets, "Role of neuro-immunological factors in the pathophysiology of mood disorders," vol. 233, ed: Psychopharmacology, 2016, pp. 1623-1636.

[17] P. Przanowski *et al.*, "The signal transducers Stat1 and Stat3 and their novel target Jmjd3 drive the expression of inflammatory genes in microglia " vol. 92, ed: Journal of Molecular Medicine, 2014, pp. 239-254.

[18] S. A. Liddelow *et al.*, "Neurotoxic reactive astrocytes are induced by activated microglia," vol. 541, ed: Nature, 2017, pp. 481-487.

[19] L. E. Clarke and B. A. Barres, "Emerging roles of astrocytes in neural circuit development," vol. 14, ed: Nature Reviews. Neuroscience., 2013, pp. 311-321.

[20] M. V. Sofroniew and H. V. Vinters, "Astrocytes: biology and pathology," vol. 119, ed: Acta Neuropathology, 2010, pp. 7-35.

[21] T. G. Bush *et al.*, "Leukocyte infiltration, neuronal degeneration, and neurite outgrowth after ablation of scar-forming, reactive astrocytes in adult transgenic mice," vol. 23, ed: Neuron, 1999, pp. 297-308.

[22] Z. Zador, S. Stiver, V. Wang, and G. Manley, "Role of aquaporin-4 in cerebral edema and stroke," vol. 190, ed: Handbook of Experimental Pharmacology, 2009, pp. 159-170.

[23] K. I. Mosher and T. Wyss-Coray, "Microglial dysfunction in brain aging and Alzheimer's disease," vol. 88, ed: Biochemical Pharmacology, 2014, pp. 594-604.

[24] M. L. Block, L. Zecca, and J. S. Hong, "Microglia-mediated neurotoxicity: uncovering the molecular mechanisms," vol. 8, ed. Nature Review Neuroscience: Nature Review. Neuroscience., 2007, pp. 57-69.

[25] M. Neal *et al.*, "Prokineticin-2 promotes chemotaxis and alternative A2 reactivity of astrocytes," vol. 66, ed: GLIA, 2018, pp. 2137-2157.

[26] R. P. Weinberg *et al.*, "Palm Fruit Bioactives modulate human astrocyte activity in vitro altering the cytokine secretome reducing levels of TNFα, RANTES and IP-10," vol. 8, ed: Scientific Reports, 2018, 16423.

[27] C. Xing, W. Li, W. Deng, M. Ning, and E. H. Lo, "A potential gliovascular mechanism for microglial activation: differential phenotypic switching of microglia by endothelium versus astrocytes," vol. 15, ed: Journal of Neuroinflamation, 2018, 143.

[28] S. A. Liddelow and B. A. Barres, "Reactive Astrocytes: Production, Function, and Therapeutic Potential," vol. 46, ed: Immunity, 2017, pp. 957-967.

[29] M. Bros, J. Boissel, U. Godtel-Armbrust, and U. Forstermann, "The untranslated region of exon 2 of the human neuronal nitric oxide synthase (NOS1) gene exerts regulatory activity," vol. 405, ed: Gene, 2007, pp. 36-46.

[30] S. Hunot *et al.*, "Nitric oxide synthase and neuronal vulnerability in Parkinson's disease," vol. 72, ed: Neuroscience, 1996, pp. 355-363.

[31] S. Love, "Oxidative stress in brain ischemia," vol. 9, ed: Brain Pathology, 1999, pp. 119-131.

[32] G. Simic *et al.*, "nNOS expression in reactive astrocytes correlates with increased cell death related DNA damage in the hippocampus and entorhinal cortex in Alzheimer's disease," vol. 165, ed: Experimental Neurology, 2000, pp. 12-26.

[33] M. V. Catania, E. Aronica, B. Yankaya, and D. Troost, "Increased expression of neuronal nitric oxide synthase spliced variants in reactive astrocytes of amyotrophic lateral sclerosis human spinal cord," vol. 21, ed: Journal of Neuroscience, 2001, RC148.

[34] G. Elain, K. Jeanneau, A. Rutkowska, A. K. Mir, and K. K. Dev, "The Selective Anti-IL17A Monoclonal Antibody Secukinumab (AIN457) Attenuates IL17A-Induced Levels of IL6 in Human Astrocytes," vol. 62, ed: GLIA, 2014, pp. 725-735.

[35] T. B. Martins *et al.*, "Analysis of Proinflammatory and Anti-Inflammatory Cytokine Serum Concentrations in Patients With Multiple Sclerosis by Using a Multiplexed Immunoassay," vol. 136, ed: American Journal of Clinical Pathology, 2011, pp. 696-704.

[36] H. T. Lee *et al.*, "Transcription-related element gene expression pattern differs between microglia and macrophages during inflammation," vol. 63, ed: Inflammation Research, 2014, pp. 389-397.

[37] Y. He, N. Taylor, L. Fourgeaud, and A. Bhattacharya, "The role of microglial P2X7: modulation of cell death and cytokine release " vol. 14, ed: Journal of Neuroinflammation, 2017, 135.

[38] A. H. Wrede, A. Shah, M. C. McNamara, R. Montazami, and N. N. Hashemi, "Controlled positioning of microbubbles and induced cavitation using a dualfrequency transducer and microfiber adhesion techniques," vol. 43, ed: Ultrasonics Sonochemistry, 2018, pp. 114-119.

[39] F. Sharifi, D. Kurteshi, and N. Hashemi, "Designing Highly Structured Polycaprolactone Fibers using Microfluidics," vol. 61, ed: Journal of the Mechanical Behavior of Biomedical Materials, 2016, pp. 530-540.

[40] Z. Bai, J. M. Mendoza Reyes, R. Montazami, and N. Hashemi, "On-Chip Development of Hydrogel Microfibers from Round to Square/Ribbon Shape," vol. 2, ed: Journal of Materials Chemistry A, 2014, pp. 4878-4884.

[41] S. Sun, J. Kanagaraj, L. Cho, D. Kang, S. Xiao, and M. Cho, "Characterization of Subcellular Responses Induced by Exposure of Microbubbles to Astrocytes," vol. 38, ed: Journal of Neurotrauma, 2015, pp. 1-8.

[42] F. Sharifi, B. B. Patel, A. K. Dzuilko, R. Montazami, D. S. Sakaguchi, and N. Hashemi, "Polycaprolactone Microfibrous Scaffolds to Navigate Neural Stem Cells," Biomacromolecules, vol. 17, 2016, pp. 3287-3297.

[43] B. B. Patel, F. Sharifi, D. P. Stroud, R. Montazami, N. N. Hashemi, and D. S. Sakaguchi, "3D Microfibrous Scaffolds Selectively Promotes Proliferation and Glial Differentiation of Adult Neural Stem Cells: A Platform to Tune Cellular Behavior in Neural Tissue Engineering," vol. 18, ed: Macromolecular Bioscience, 2018, 1800236.

[44] K. J. Livak and T. D. Schmittgen, "Analysis of relative gene expression data using real-time quantitative PCR and the 2(-Delta Delta C(T)) Method," vol. 25, ed: Methods, 2001, pp. 402-408.

[45] M. B. Panzer, B. S. Myers, B. P. Capehart, and C. R. Bass, "Development of a finite element model for blast brain injury and the effects of CSF cavitation," vol. 40, ed: Annals of Biomedical Engineering, 2012, pp. 1530-1544.

[46] J. L. Zamanian *et al.*, "Genomic Analysis of Reactive Astrogliosis," vol. 32, ed: Journal of Neuroscience, 2012, pp. 6391-6410.

CHAPTER 5. LONGITUDINAL GENETIC STUDY OF REACTIVE ASTROCYTES INDUCED BY NEARBY CAVITATION

Modified from a manuscript submitted in ACS Nano

Alex H. Wrede[1], Jie Luo[2], Reza Montazami[1], Anumantha Kanthasamy[2], and Nicole N. Hashemi[1,2]*

[1] Department of Mechanical Engineering, Iowa State University, Ames, Iowa 50011, USA

[2] Department of Biomedical Sciences, Iowa State University, Ames, IA 50011, USA

Abstract

Reactive astrocytes are known to play a vital role in the overall response of the brain during a traumatic brain injury (TBI). Modern studies have speculated the existence of cavitation in the skull during a TBI, which has alarming potential to cause detrimental damages. Previous studies have confirmed the upregulation of various harmful genes in neurodegenerative diseases. Studying the longitudinal presence of these harmful genes in response to cavitation allows for optimized understanding and treatment methods in cavitation exposure. We seek to characterize the longitudinal genetic expression levels that astrocytes exhibit after exposure to cavitation and further elucidate the startling presence of cranial cavitation. Astrocytic expression levels of various common genes that have been documented in TBI research are our target of interest, like, TNFα, IL-1β, and NOS1. Results summarize specific gene trends from 1-48 hours after cavitation. Our data concludes that maximum expression is not consistently exhibited

immediately after cavitation exposure, and most genes have individualized genetic trends. IL-1β shows a decreasing expression over 48 hours, and TNFα shows upregulation until the 6 hour time point but then begins to decrease in expression. The upregulation of NOS1 has been documented in neurodegenerative diseases, like Alzheimer's and Parkinson's disease. This study has shown a consistent upregulation in NOS1 expression from 0-48 hours. These results postulate a possible linkage between cavitation damage and neurodegenerative diseases. This analysis also provides novelty in optimizing treatments for astrocytic function post-TBI and legitimizing the concern of cranial cavitation existence. These results add motivation for future studies of cavitation elimination or minimization via advanced helmet and airbag engineering.

5.1 Introduction

Despite an abundance of recent efforts in TBI research, there are still undiscovered attributes in the neuronal response to these situations. Reactive astrocytes play a vital role in a variety of neurodegenerative diseases, including Alzheimer's disease and Parkinson's disease[1-3]. Previous studies have shown that the effects from altered astrocytic gene expression is dependent on the specific inducer of the trauma, adding an increased level of complexity in TBI response characterization. For example, ischemia induced astrocytic change represents a genetic phenotype that is beneficial and sustaining to surrounding neuronal anatomy. On the contrary, an inflammatory exposure, like lipopolysaccharide (LPS), induced astrocytes that cause detrimental gene alterations[4].

For simplicity, scientists have categorized detrimental reactive astrocytes as 'A1' astrocytes and protective reactive astrocytes as 'A2' astrocytes[3]. Ischemia and LPS are two possible exposures that will induce reactive astrocytes, but it remains a question as to how

reactive astrocytes respond differently to other types of TBI exposures. A modern theory postulates that a likely inducer of reactive astrocytes following a blast-TBI is the presence of cavitation[5].

Cavitation is a byproduct of low pressure regions in the brain, which are a result from an initial compressive wave reflecting off the opposite side of the skull[6, 7]. The localized force from cavitation leaves behind profound damages in other applications, like boat propeller and hydrodynamic pump erosion[8, 9]. Understanding whether surrounding cavitation exposure produces A1s, A2s, or a combination of each, is critical in order to further unmask the complexity of TBIs. Previous research has analyzed the specific astrocytic gene expression alterations immediately after experiencing surrounding cavitation. These results showed an upregulation in a number of classic A1 specific genes, including TNFα, IL-1β, C1q, Serping1, NOS1, and IL-6. Results showed minimal changes in classic A2 specific genes with the exception of CD14[10].

In this study, we expand on previous methods to conduct a longitudinal study that specifically elucidates astrocytic gene expression abnormalities over time, after experiencing exposure to surrounding cavitation. It is known that gene expressions can change over time and further characterizing this trend in reactive astrocytes has great potential[4], like leading to advanced pharmaceutical techniques to restore altered cellular function. This study analyzes the astrocytic gene expressions up to 48 hours post-cavitation exposure via quantitative polyermase chain reaction methods (qPCR) methods. These genetic analytics yield insight on the behaviors that reactive astrocytes exhibit after exposure to nearby cavitation and provide a foundation of knowledge that helps further characterize reactive astrocytic nature in TBIs.

5.2 Materials and Methods

5.2.1 Cell Model

Mouse astrocytes (CRL-2541, ATCC, Manassas, VA) are solely used in this project because of their documented utility in TBI studies[11, 12]. The astrocytes were cultured according to company protocol in base media (ATCC, 30-2002). The growth media was also composed of 10% FBS and 1% penicillin (10,000 U/mL)- streptomycin (10,000 µg/mL) (Gibco, Waltham, MA). All cells in this study were from culture passage numbers 5-7. The astrocytes were stored in an incubator set with constant parameters of 37 °C and 5% CO_2. The mouse astrocytes were seeded into the 6-plates at a concentration of $9.04 * 10^6$ cells per well and stored for 24 hours in the incubator prior to experimentation.

5.2.2 Apparatus Configuration and Methodology

The method of creating controlled cavitation is similar to that of previous studies[13]. The main difference in the apparatus configuration of this experiment is the cells are seeded onto sterilized 6-well culture plates instead of using microfiber scaffolds, shown in Figure 5.1. All components are housed in a 1.5 gallon tank filled with phosphate buffered saline (PBS). During trials, the experimental samples are directed downward toward capillary tubing (Polymicro Technologies, 1068150003) that is continuously releasing microbubbles (MBs) ~60µm in diameter at a rate of ~150 MBs/min. The 6-well plate is mounted on a 3-axis adjustable stage (MT1, Thor Labs, Newton, New Jersey) allowing for MBs to adhere arbitrarily across the cell-seeded surface. After a 350-400 MBs are adhered to each well the culture plate is then rotated 180°, exposing the astrocyte-MB complex to a 100 kHz transducer positioned overhead in the tank. The transducer induces resonant conditions causing the MBs to oscillate and fragment, also

known as induced cavitation (center frequency 100 kHz, 5 cycles, pulse repetition frequency 59 Hz, 260 Vpp). The frequency signal is amplified using a broadband power amplifier (E&I, 1140LA). The control samples were introduced to an interchangeable environment, but they did not experience nearby cavitation because there were not any MBs arbitrarily captured in these wells.

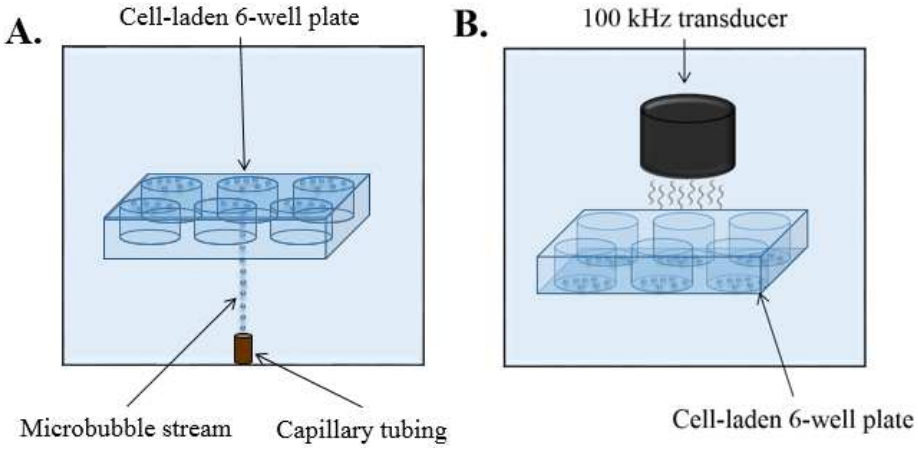

Figure 5.1: Apparatus layout of MB capturing and induced cavitation on cell-laden 6-well plates. (A) 350-400 MBs are captured and adhered to the bottom of all the cell-laden culture wells. (B) The 6-well plate is rotated 180° and exposed to the 100 kHz transducer. The transducer is centered above each well individually. When the transducer is turned on the astrocytes are introduced to surrounding cavitation.

A full 6-well plate was designated for a specific time point, three wells for experimental samples and 3 wells for control samples. Designating one plate for each time point was advantageous because the experimental and control samples experienced exact amounts of PBS and ultrasound exposure with this orientation. Another advantage of this setup is the ability to retain cells that detached from the well due to the cavitation force. When the cells detach they drift within the boundaries of each specific well, allowing them to be part of the post-cavitation analysis. Previous methods use cell-laden coverslips without ridges so the detached cells are unable to be collected[10]. After the plate was pulled from the tank, the remaining PBS solution

was pipetted out and replaced with fresh growth media. The pipetted PBS was centrifuged at 1500 rpm for five minutes to collect all the detached cells. The pelleted cells were put back in the original wells and placed in the incubator until its specific designated time point after exposure. Astrocyte response was studied 1 hour, 3 hours, 6 hours, 12 hours, 24 hours, and 48 hours after cavitation exposure.

5.2.3 Gene Expression Analysis via qPCR

The cell-laden 6-well plates were trypsinized and combined to create one control and one experimental sample at each designated time point. Each sample was then centrifuged at 1500 rpm for 5 minutes to pellet the cells. The cell pellet was broken with TRIzol reagent (Invitrogen Cat number: 15596026) and frozen at -80 °C until all time points were resuspended. Homogenization was done in TRIzol RNA isolation and specifically conducted following the TRIzol reagent protocol from the manufacturer. The entirety of the qPCR process in obtaining relative gene expression values is consistent with that of previous studies[10, 14].

5.3 Results and Discussion

Longitudinal gene expression analysis has been done on both A1 and A2 genes from 1-48 hours. Figure 5.2 highlights the expression trends for A1 genes, including, Serping1, C1q, TNFα, NOS1, IL-6, and IL-1β. All data is represented as a fold change that is normalized to a control sample that was absent of cavitation damage. This data collection is an exploratory approach to elucidate any noticeable trends in expression values. Combining these trends with previous data that quantitates the expressions immediately after cavitation allows for a full 48 hour timeline[10].

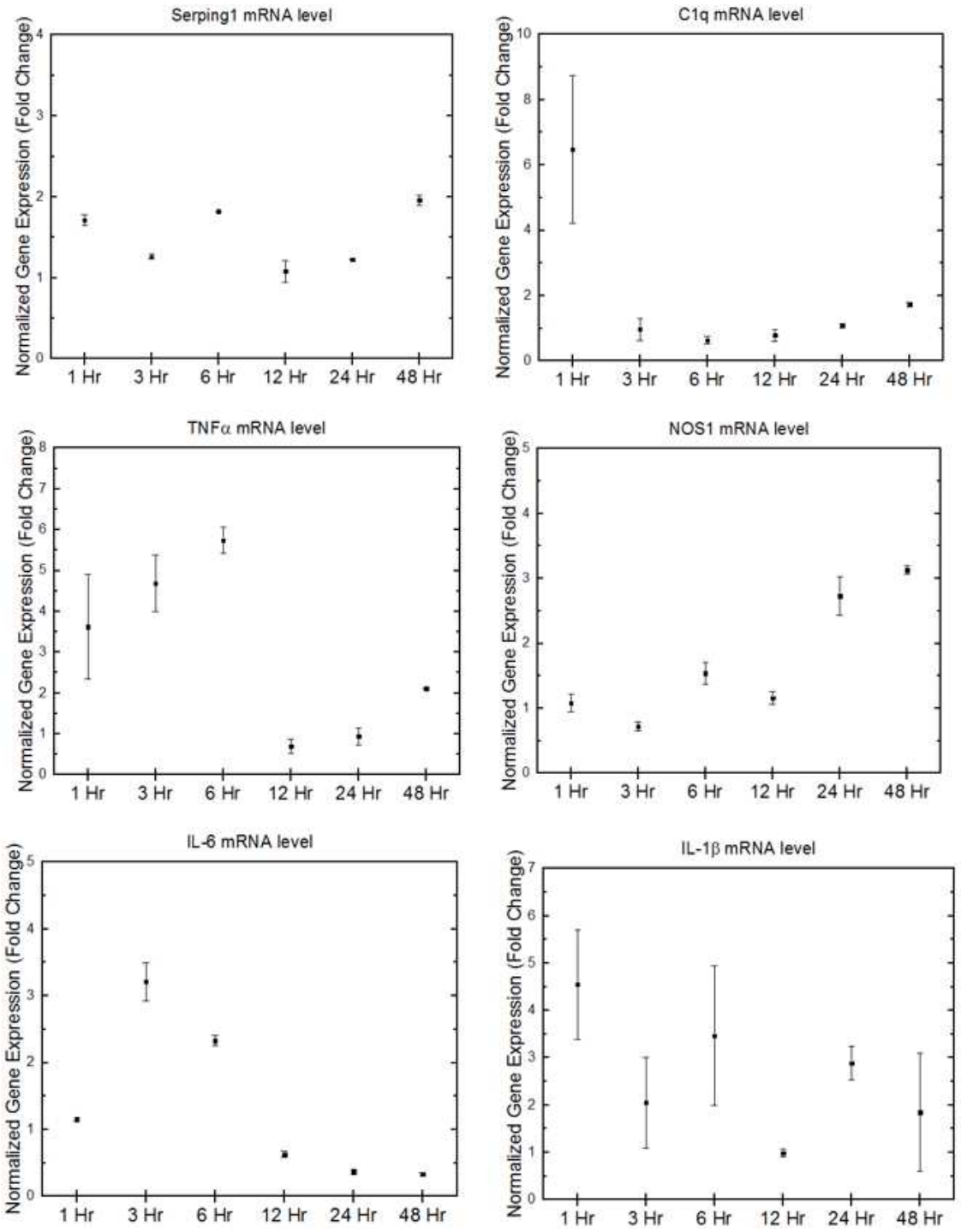

Figure 5.2: Longitudinal gene expression summaries of A1 genes. Error bars represent standard error of the mean.

Previous data found Serping1, IL-1β, and C1q having a +5 fold change immediately after cavitation[10]. Figure 5.1 illustrates Serping1, IL-1β, and C1q all decreasing with time over 48 hours. Serping1 decreases rapidly and is shown to consistently remain within a 1-2 fold change from 1-48 hours. C1q shows similar trends with the exception of a significant upregulation remaining at 1 hour. IL-1β shows a decreasing trend over 48 hours but has a larger amount of variance and upregulation. TNFα and IL-6 both show upregulation over the first time points but at the 6 hour and 3 hour time points they begin to decrease in expression, respectively. From the A1 genes of interest, NOS1 is the only A1 gene that represents an increasing expression trend throughout 1-48 hours. A variety of neurodegenerative diseases, like Alzheimer's and Parkinson's disease, have been linked to upregulation of NOS1[2]. The nature and symptoms from these diseases also escalate over time, ultimately motivating a hypothesis that directly associates cavitation exposure with Alzheimer's and Parkinson's disease. Although this is only one gene trend, these results raise concern and motivate future studies to elucidate the linkage between cavitation and specific neurodegenerative diseases.

Figure 5.3 summarizes the gene expression trends for some A2 genes, including, tm4sf1, sphk1, CD14, and Arginase1. The overall trends of sphk1 and Arginase1 represent similar patterns, increasing in expression until peaking at 6 hours and showing a ≤ 1 fold change thereafter. Previous data concluded CD14 having +5 fold change immediately after cavitation[10]. This study demonstrates an overall trend of CD14 decreasing with time. Tm4sf1 shows consist expressions compared to the control, with the exception of a +2 fold change at 24 hours.

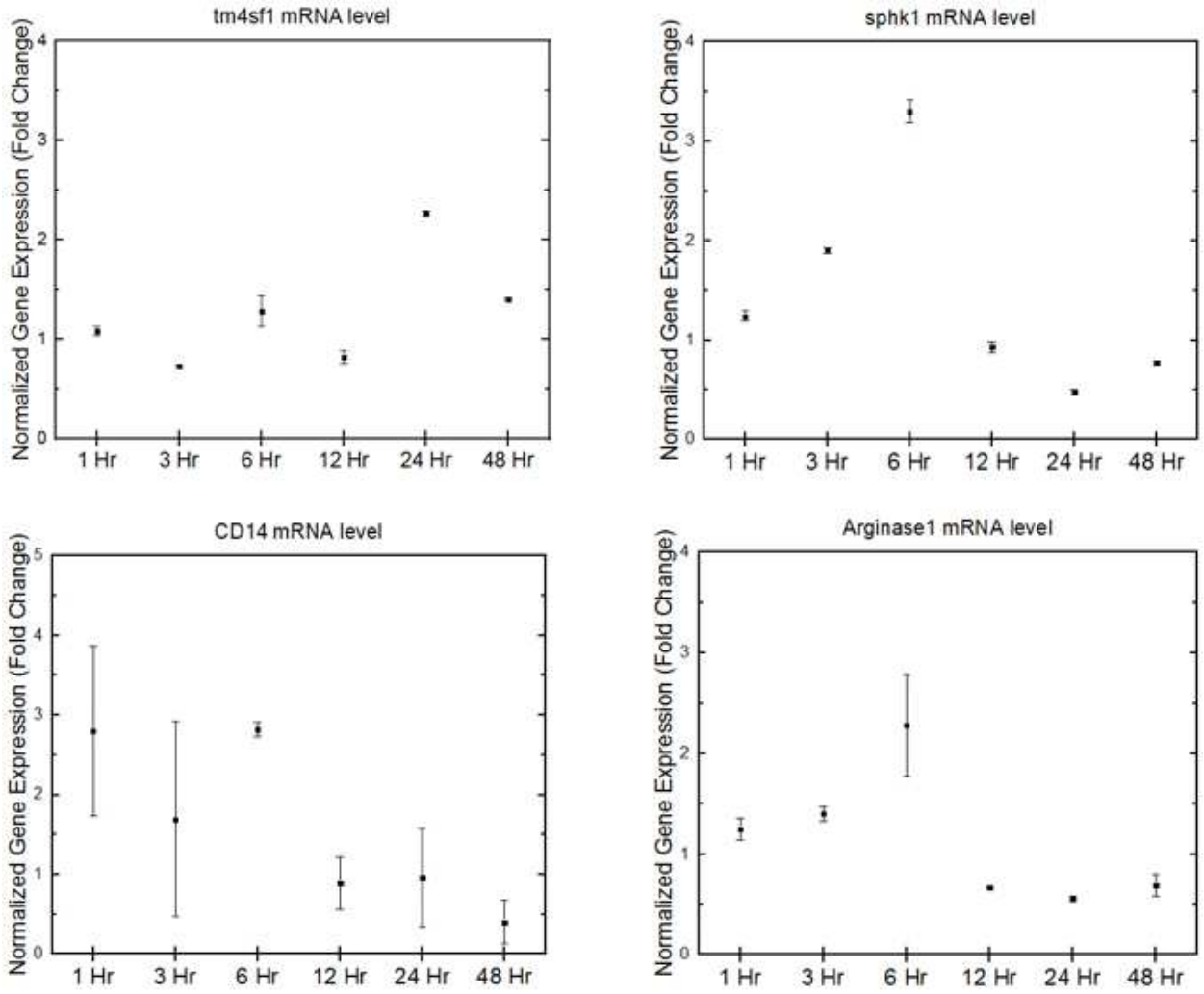

Figure 5.3: Longitudinal gene expression summaries of A2 genes. Error bars represent standard error of mean.

This exploratory study has illustrated the unique response that cavitation induces on various A1 and A2 genes. These are the beginning trials of this investigation and future research aims to conduct RNA sequencing analytics to highlight larger groupings in the entire genome that experience expression alterations. The selected genes of this study were chosen based off of significance in existing literature. RNA sequencing will expose additional groups of genes that are of interest. Postulating a method of treatment has some value with the collected data of this

study, but it is important to remember that cavitation is one of multiple injuries that occur during a TBI. Studying the genetic trends from overall TBI exposure has been heavily researched and treatment techniques have been proposed[15]. The genetic responses gathered in this study help raise awareness of the distinct changes that astrocytes undergo from solely cavitation exposure. The conditions in which cavitation likely exists in the human skull is, for the most part, unknown so we are proposing further studies that focus on characterizing the parameters that allow cavitation to exist in a TBI situation. The ultimate goal would be to take the parameter limits and engineer helmets and automotive airbags to keep the conditions within the skull from reaching these thresholds. Using these proposed parameter limits in conjunction with the longitudinal results from this study, treatments can be given at the optimized time point to assist in cranial recovery if the skull was simulated through a cavitation-inducing environment. All in all, cavitation existing in the skull urges the motivation for many future studies. The longitudinal genetic trends in this study are novel in helping piece together the complexity of the unique response that the brain has to cavitation.

5.4 Conclusion

Optimizing the specific diagnosis and care for TBIs is currently a major challenge. This is due to the fact that TBIs are a complex injury that have a variety of parameters to account for. Recent studies have added an additional layer to this puzzle with the idea that cavitation exists inside the skull during a TBI. Studying the response that neuronal anatomy has to this event is vital in optimizing TBI diagnosis and care. This study has documented the longitudinal gene expression trends that exist in a number of common A1 and A2 genes. Results have shown that each A1 and A2 gene of interest has a unique expression response and peaks at varying time

points. Treatments should be optimally given prior to the discovered peaks of the A1 genes to reduce damages that are known to be present in neurodegenerative diseases. These findings are novel in the progression of TBI knowledge and help illustrate more of the nature in the response of the brain in TBI situations. Future studies aim to expand on these results and gather complete genome trends.

References

[1] R. M. Ransohoff and J. E. Khoury, "Microglia in Health and Disease," vol. 8, ed: Cold Spring Harbor Perspectives in Biology, 2015, p. 1.

[2] A. Bhattacharya, N. C. Derecki, T. W. Lovenberg, and W. C. Drevets, "Role of neuro-immunological factors in the pathophysiology of mood disorders," vol. 233, ed: Psychopharmacology, 2016, pp. 1623-1636.

[3] S. A. Liddelow *et al.*, "Neurotoxic reactive astrocytes are induced by activated microglia," vol. 541, ed: Nature, 2017, pp. 481-487.

[4] J. L. Zamanian *et al.*, "Genomic Analysis of Reactive Astrogliosis," vol. 32, ed: Journal of Neuroscience, 2012, pp. 6391-6410.

[5] C. Franck, "Microcavitation: the key to modeling blast traumatic brain injury?," vol. 2, ed: Concussion, 2017, p. 3.

[6] R. S. Salzar, D. Treichler, A. Wardlaw, G. Weiss, and J. Goeller, "Experimental Investigation of Cavitation as a Possible Damage Mechanism in Blast-Induced Traumatic Brain Injury in Post-Mortem Human Subject Heads," vol. 34, ed: Journal of Neurotrauma, 2017, pp. 1589-1602.

[7] S. Canchi, K. Kelly, Y. Hong, M. A. King, G. Subhash, and M. Sarntinoranont, "Controlled single bubble cavitation collapse results in jet-induced injury in brain tissue," vol. 74, ed: Journal of the Mechanical Behavior of Biomedical Materials, 2017, pp. 261-273.

[8] Z.-f. Zhu and S.-l. Fang, "Numerical investigation of cavitation performance of ship propellers," vol. 24, ed: Journal of Hydrodynamics, 2012, pp. 347-353.

[9] L. Chernin and D. V. Val, "Probabilistic prediction of cavitation on rotor blades of tidal stream turbines," vol. 113, ed: Renewable Energy, 2017, pp. 688-696.

[10] A. H. Wrede, M. C. McNamara, J. Luo, R. Montazami, A. Kanthasamy, and N. N. Hashemi, "Characterization of Astrocytic Response after Experiencing Cavitation In vitro," ed: Global Challenges, 2019.

[11] S. Sun, J. Kanagaraj, L. Cho, D. Kang, S. Xiao, and M. Cho, "Characterization of Subcellular Responses Induced by Exposure of Microbubbles to Astrocytes," vol. 38, ed: Journal of Neurotrauma, 2015, pp. 1-8.

[12] H. Jang *et al.*, "Hydrogen Sulfide Treatment Induces Angiogenesis After Cerebral Ischemia," vol. 92, ed: Journal of Neuroscience Research, 2014, pp. 1520-1528.

[13] A. H. Wrede, A. Shah, M. C. McNamara, R. Montazami, and N. N. Hashemi, "Controlled positioning of microbubbles and induced cavitation using a dualfrequency transducer and microfiber adhesion techniques," vol. 43, ed: Ultrasonics Sonochemistry, 2018, pp. 114-119.

[14] K. J. Livak and T. D. Schmittgen, "Analysis of relative gene expression data using real-time quantitative PCR and the 2(-Delta Delta C(T)) Method," vol. 25, ed: Methods, 2001, pp. 402-408.

[15] Y. H. Chen *et al.*, "Rapamycin improves the neuroprotection effect of inhibition of NLRP3 inflammasome activation after TBI," vol. 1710, ed: Brain Research, 2019, pp. 163-172.

CHAPTER 6. FUTURE WORK

It is known that when astrocytes enter a reactive state they change morphologically [1]. Morphological studies have been conducted in previous chapters to visually analyze the longitudinal structural changes of the astrocytes over time. Additional future studies seek to use microfluidic chips to sort cells based on their size. These microfluidic chips have optimized dimensions and groove patterns to deflect cells differently based on their morphological size. Theoretically cells that experience cavitation likely represent a smaller size because they show an amoeboid morphology when they are stunned or damaged. These cells will likely deflect in the microfluidic channels more than undamaged cells and collect in wells 4&5 shown in Figure 6.1. Comparative analysis on the percent volume of sorted control and experimental samples would help elucidate distinct morphology change as a result of nearby cavitation. These microfluidic chips are also used to sort cells based on other biomechanical properties that has potential to provide additional novelty [2].

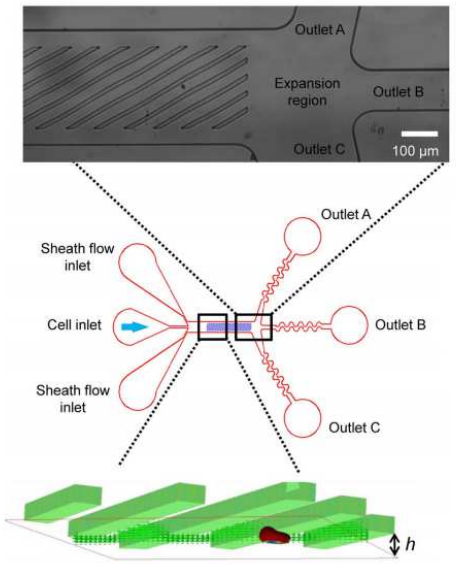

Figure 6.1: *Microfluidic mold of a size sorting cellular device [2]*.

In our genetic studies we selected genes of interest based on a literature review of gene that are present in reactive astrocytes as a result of TBIs. Using qPCR methods we were able to characterize the genetic trends in these genes after experiencing cavitation exposure. Implementing RNA sequencing on the astrocyte samples would yield additional novelty and allow for genetic insight on the complete genome. We did not have the resources to conduct these tests and we took more of an exploratory approach to see immediate expression trends in our genes of interest. Additionally, single cell RNA sequencing is a technique used to gather genomic data on small amounts of cells. This testing would be very novel to implement and use to characterize the genomic representation of the astrocytes that are seeded on PCL microfibers in chapter 4, and specifically illustrated in Figure 4.4. Because we did not have access to this type of analysis we increased the scale of cell count and implemented qPCR methods to conduct genetic analysis.

References

[1] U. Wilhelmsson *et al.*, "Redefining the concept of reactive astrocytes as cells that remain within their unique domains upon reaction to injury," vol. 103, ed: PNAS, 2006, pp. 17513-17518.

[2] G. Wang, C. Turbyfield, K. Crawford, A. Alexeev, and T. Sulchek, "Cellular enrichment through microfluidic fractionation based on cell biomechanical properties " vol. 19, ed: Microfluid Nanofluid, 2015, pp. 987-993.